It is clear that a small contribution of the σ octet, of the order of $\frac{1}{10}$ of the σ singlet one, is enough to make a perfect fit to experiment with the obvious exception of $\mathrm{Re}a_0$.

Finally we want to mention that in this model the π–π final-state interaction is still small while this is not the case for the $K\bar{K}$ one.

VI. CONCLUSIONS

The results of Sec. IV have a meaning independent of the model meson source. The connection between the subtraction constants in dispersion relations for amplitudes and equal-time commutators can be useful in many applications, particularly those in which the soft-meson limit is a good approximation. This connection gives the possibility of using the limit $k^2=q^2=0$ which is less restrictive than $k_\mu=q_\mu=0$. Moreover, now one knows better how to evaluate corrections to it through approximate calculations of the dispersive integral (Ref. 12).

The information contained in the equal-time commutators can be useful also in predicting low-energy parameters of processes not involving mesons (as NN scattering), through the knowledge of the t dependence of the subtractions in processes related by unitarity.

It would be interesting to study the connection between the high-energy, Regge-type behavior of amplitudes and the algebraic properties of weak and electromagnetic currents. These two phenomena can be strongly correlated as they independently predict the subtraction constants .[18]

ACKNOWLEDGMENTS

We are indebted to Professor Abdus Salam and Professor K. C. Wali for their continued interest in this work and to Professor J. J. Sakurai for a very interesting discussion. We are also grateful to Dr. A. Della Selva for his collaboration in the first stage of this investigation and to Dr. R. Ramachandran for many critical remarks.

It is a pleasure to thank Professors Abdus Salam and Paolo Budini and the International Atomic Energy Agency for hospitality at the International Center for Theoretical Physics, Trieste.

[18] H. R. Rubinstein and G. Veneziano, Phys. Rev. **160**, 1286 (1967).

PHYSICAL REVIEW VOLUME 166, NUMBER 5 25 FEBRUARY 1968

Phenomenological Analysis of $I=\frac{1}{2}$ Single-Pion Production Processes in the Energy Range 500 to 700 MeV

D. MORGAN

Rutherford High Energy Laboratory, Chilton, Berkshire, England

(Received 7 September 1967)

Single-pion production processes in the energy range 500 to 700 MeV are discussed. It is assumed that production occurs in the partial waves S_1, P_1, P_3, and D_3 for $I=\frac{1}{2}$ and $\frac{3}{2}$ via isobar formation in a generalized sense. Isobars treated are the $N^*(1236)$ and the low-energy tails of the σ (assumed to be a broad resonance centered at 700 MeV) and the ρ. Emphasis is laid on maintaining consistency with the results of elastic phase-shift analyses. It is suggested that the major contributor to the charge channel $\pi^0\pi^-p$ at and above 550 MeV is P_{11} decaying via ρN. It is noted that a second P_{11} resonance occurring in the range 600 to 800 MeV would explain several phenomena. It is indicated that D_{13} very probably decays to σN as well as πN^*. A plea is entered for the presentation of future data in the form of a full production-angular-distribution analysis over the Dalitz plot.

I. INTRODUCTION

IN this paper, production processes $\pi N\to\pi\pi N$ in the general energy range below 1 GeV, and especially $\pi^-p\to\pi\pi N$ between 500 and 700 MeV, are discussed. For these energies, one can attempt to delineate the roles of individual J^P states and to characterize their decay channels. A careful study of this region is of interest because it is known from the analysis of elastic scattering and photoproduction to contain several inelastic resonances, P_{11}, D_{13}, and S_{11}. One wants to know the inelastic modes of these resonances—to what extent they are coupled to πN^*, to what extent to a final state comprising a nucleon and the enigmatic $I=0$ S-wave $\pi\pi$ system, and so on.

A very extensive analysis of single-pion production below 1 GeV has been given by Olsson and Yodh[1,2] (OY) and a number of other analyses have been published.[3–6] There is a large literature on techniques. The object of the present paper is to reassess some of the conclusions which can be reached from existing data

[1] M. Olsson and G. B. Yodh, Phys. Rev. **145**, 1309 (1966).
[2] M. Olsson and G. B. Yodh, Phys. Rev. Letters **10**, 353 (1963); University of Maryland Technical Report Nos. 358 (1964) and 512 (1965) (unpublished); Phys. Rev. **145**, 1327 (1966).
[3] J. M. Namyslowski, M. S. K. Razmi, and R. G. Roberts, Imperial College, London, Report No. ICTP/65/20 (unpublished); Phys. Rev. **157**, 1328 (1967).
[4] P. G. Thurnauer, Phys. Rev. Letters **14**, 985 (1965); University of Rochester Report No. UR-875-119, 1966 (unpublished).
[5] B. Deler and G. Valladas, Nuovo Cimento **45A**, 559 (1966).
[6] A. Courau, Nuovo Cimento **41**, 261 (1966).

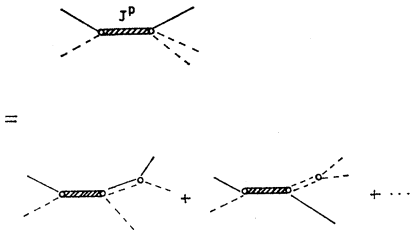

FIG. 1. Schematic of the isobar model.

and to emphasize certain features which should be looked for in the new higher-statistics experiments which are currently being performed.

The conceptual framework of our analysis is as follows: (i) separate the production amplitude into partial-wave production amplitudes for particular J^P states, and (ii) attempt to interpret these via the isobar model as a sum of terms T_α for which the pair α undergoes final-state interactions (Fig. 1).

In order to learn which J^P states are important, one looks at the elastic phase-shift analyses and also at evidence from the production processes, in particular at production angular distributions. To learn which decay channels are important, one again studies the production data, especially Dalitz plots and effective mass spectra. One attempts to fit the data to an isobar model in which particle pairs which are known or believed to interact strongly form the isobars.

The partial waves considered are $\frac{1}{2}^-(S_1)$, $\frac{1}{2}^+(P_1)$, $\frac{3}{2}^+(P_3)$, and $\frac{3}{2}^-(D_3)$ for $I=\frac{1}{2}$ and $\frac{3}{2}$. The isobars taken into account are primarily $N^*(1236)$, the $I=0$, $J=0$ $\pi\pi$ state denoted by σ (this without prejudice as to whether there is a σ resonance in the energy range of interest or at all), and the $I=1$, $J=1$ $\pi\pi$ state denoted by ρ (the relevant dipion energies are of course well below the ρ mass).

Existing data are not sufficient to distinguish fully between all the alternatives open; still less to force one beyond the confines of the isobar model. Nonetheless, certain tentative conclusions can be reached. In particular, one is led to a somewhat different apportionment of the effects due to the D_{13} and P_{11} resonances from that deduced in the OY analysis.[1] The new features are as follows: (1) A different charge branching ratio of D_{13} and P_{11} into the channels $\pi^0\pi^- p$, $\pi^+\pi^- n$ and $\pi^0\pi^0 n$ is found. (2) It is suggested that the P_{11} system at and above 550 MeV is strongly coupled to the ρN final state. (3) It is noted that a second P_{11} resonance occurring in the range 600 to 800 MeV is not ruled out by the elastic phase-shift analyses and would be helpful in explaining some of the production phenomena.[6a] (4) Examination of the Dalitz plot distribution for $\pi^- p \to \pi^+\pi^- n$ indicates the presence in D_{13} of a component decaying to σN as well as the usual πN^* mode.

We are led to differ in the above respects through stressing (a) the need to maintain approximate agreement with the elastic phase-shift results; (b) the data on production angular distributions.

Such conclusions on the P_{11} and D_{13} are persuasive rather than compelling and the role of production via other J^P states is uncertain. We stress the desirability of presenting future data in the form of a full production angular distribution analysis over the Dalitz plot.

The main portion of the paper is Sec. V. In Sec. II, the angular momentum formalism is outlined and further details are given in Appendix A. The theoretical basis of the isobar model is sketched in Sec. III and the specific model employed in the present analysis described in Sec. IV. Section V is devoted to the discussion of the data and Sec. VI to conclusions. Formulas for the analysis of production angular distributions are derived in Appendix B.

II. ANGULAR MOMENTUM FORMALISM

We now summarize some of the formalism for production amplitudes which has been developed by various authors[3–5,7–10] in order to establish notation and conventions. Further details are given in Appendix A.

The production amplitude for a process 2 bodies $\to$ 3 bodies with given helicities depends on five kinematic variables. These can conveniently be taken to be the square of the total energy, $s=E^2$, two production angles Θ,Φ, for example, the polar coordinates of the incoming particle direction with respect to the production plane in the over-all c.m. system, and the two coordinates of Dalitz plot say ω_1, ω_2 (definition below). Through angular momentum decomposition, one can express the total production amplitude as a sum in terms of partial-wave production amplitudes depending on the three variables (s,ω_1,ω_2). These partial-wave amplitudes can, if desired, be further decomposed into states where one of the two-body subsystems has definite angular momentum by using the linear relation between appropriate coordinates on the Dalitz plot and cosines of decay angles. The second decomposition is necessary to give a simple form to final-state interactions and the isobar model.

We define the following three-vectors and scalars: $\mathbf{q}_i$=momentum of final particle i in the over-all c.m. system ($\sum \mathbf{q}_i=\mathbf{0}$ by definition). [The index i is assumed always to run over the values 1, 2, 3; (ijk) denotes a permutation of (1 2 3). We adopt the convention for discussing the $\pi\pi N$ system that particles 1 and 2 are pions with charge of $1\geqslant$ charge of 2; particle 3 is the nucleon.] $\mathbf{n}$=unit normal to the production plane. $\omega_i=(m_i^2+q_i^2)^{1/2}$ is the total energy of particle i, mass m_i [$\sum \omega_i=E=\sqrt{s}$]. $\mathbf{q}_A$=incoming momentum in the

[6a] *Note added in proof.* A second P_{11} resonance of mass 1751 MeV has been proposed by A. Donnachie *et al.*, Phys. Letters **26B**, 161 (1968).

[7] G. C. Wick, Ann. Phys. (N. Y.) **18**, 65 (1962).

[8] D. Branson, P. V. Landshoff, and J. C. Taylor, Phys. Rev. **132**, 902 (1963); to be referred to as BLT.

[9] S. M. Berman and M. Jacob, Phys. Rev. **139**, B1023 (1965).

[10] R. C. Arnold and J. L. Uretsky, Phys. Rev. **153**, 1443 (1967), to be referred to as AU.

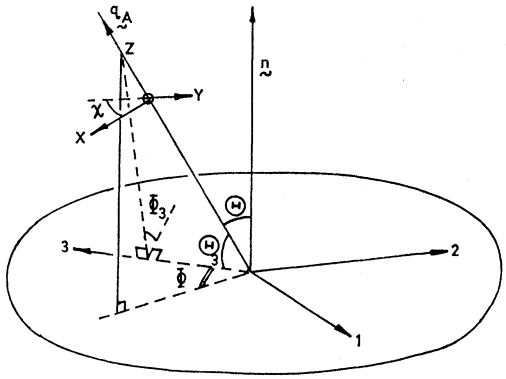

FIG. 2. Angular variables for the analysis of processes $2 \to 3$. $\mathbf{q}_A$ is the incoming particle momentum; 1, 2, 3 are the outgoing particle directions; OX, OY, OZ are space-fixed axes.

over-all c.m. frame. $\mathbf{q}_{ij}$= relative momentum of particles i and j in the c.m. frame of the two-body (ij) susbystem. (This is obtained from the over-all c.m. frame by applying a Lorentz transformation in the direction $\mathbf{q}_k$.) $\omega_{ij}^2=(\omega_i+\omega_j)^2-(\mathbf{q}_i+\mathbf{q}_j)^2$= invariant mass squared of ij subsystem.

$$[\omega_{12}^2+\omega_{23}^2+\omega_{31}^2=s+m_1^2+m_2^2+m_3^2,$$
$$\omega_{23}^2=E^2+m_1^2-2E\omega_1, \text{ etc.}]$$

We write $|\mathbf{q}_i|=q_i$ and denote by $\hat{q}_i$ the unit vector $\mathbf{q}_i/q_i$ and similarly for the other vectors.

Angles Θ, Φ, Θ_i, Ψ, θ_i, χ_i are defined in Appendix A and Figs. 2, 3. In terms of these and the other kinematic quantities introduced above a number of alternative specifications of three-body states can be given. The quantities (Ψ,Θ,Φ) or (Ψ,Θ_i,Φ_i) constitute sets of Euler angles to specify the orientation in space of the production plane. The θ_i and χ_i are the functions on the Dalitz plot, θ_i is the angle between $\hat{q}_{jk}$ and $\hat{q}_i$ and χ_i the angle between $\hat{q}_j$ and $\hat{q}_k$.

The orientations of intrinsic spin may be specified in one of the following ways: (i) helicities in the over-all c.m. system denoted by μ_i; (ii) transversities[11] in the over-all c.m. system denoted by λ_i, i.e., components of spin along the normal to the production plane; (iii) helicities in the (ij) subsystem c.m. frame denoted by ν_i.

(i) and (ii) are related by the appropriate rotations connecting the quantization axes. (i) and (iii), which involve helicity transformations between different Lorentz frames, are connected by the Wick rotations.[7] As discussed in Appendix A, it is a reasonable approximation for the energy range of the present discussion to take the nonrelativistic form for the Wick angles. The Wick rotations then also appear as rotations connecting the quantization axes. This enables us to use nonrelativistic tensorial expressions involving Pauli spin matrices to express the angular dependence of production amplitudes [see Eq. (4.5) below].

[11] A. Kotánski, Acta Phys. Polon. **29**, 699 (1966); **30**, 629 (1966).

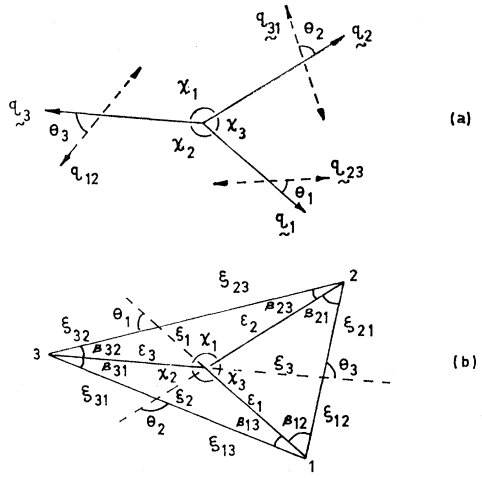

FIG. 3. (a) Angles and vectors in the production plane. (b) The Wick triangle (spherical triangle).

Following BLT[8] and AU,[10] we define the production amplitude $T_\lambda^m(s,\omega_1,\omega_2;\Phi,\Theta,\Psi)$. Here, m denotes the initial nucleon helicity and λ the final nucleon transversity. The production cross section is defined to be

$$\frac{\partial^4\sigma(m,\lambda)}{\partial\omega_1\partial\omega_2\partial(\cos\Theta)\partial\Phi}=\frac{\pi^3}{16E^3q_A}|T_\lambda^m|^2. \quad (2.1)$$

The angular decomposition of T_λ^m is given by the formula

$$T_\lambda^m(s,\omega_1,\omega_2;\Phi,\Theta,\Psi)=\sum_{J=1/2}^{\infty}\sum_{\Lambda=-J}^{+J}\left(\frac{2J+1}{4\pi}\right)^{1/2}$$
$$\times D_{\Lambda m}^J(\Phi,\Theta,\Psi)T_{J\Lambda}^{m\lambda}(s,\omega_1,\omega_2). \quad (2.2)$$

Here, Λ denotes the total transversity of the final state (component of the total angular momentum J along the normal to the plane of production). The quantities (Φ,Θ,Ψ) constitute the Euler angles defining the rotation from space-fixed axes to a possible set of body-fixed axes, in this case the normal set with Z axis perpendicular to the production plane. There exist alternative decompositions based on the Euler sets (Φ_i,Θ_i,Ψ) which correspond to taking the direction $\mathbf{q}_i$ as Z axis. The magnetic substate components of the two representations are connected by the appropriate rotation matrices. In order to proceed to the second angular momentum decomposition, we suppose such a transformation to have been made and write for example

$$T_{\mu_3}^m(s,\omega_1,\omega_3;\Phi_3,\Theta_3,\Psi)=\sum_{J=1/2}^{\infty}\sum_{\mu=-J}^{J}\left(\frac{2J+1}{4\pi}\right)^{1/2}$$
$$\times D_{\mu m}^J(\Phi_3,\Theta_3,\Psi)T_{J\mu}^{=\mu_3}(s,\omega_{12}^2,\cos\theta_3). \quad (2.3)$$

Here we have chosen the nucleon direction $\mathbf{q}_3$ as OZ and have taken as Dalitz-plot coordinates ω_{12}^2, $\cos\theta_3$. We

can now use the unit projection operators developed in Appendix A to make the second decomposition:

$$T_{J\mu}{}^{m\mu_3}(s,\omega_{12}{}^2,\cos\theta_3)=\sum_{j_{12}=0}^{\infty}\sum_{m_{12}}(2j_{12}+1)^{1/2}2(4\pi)^{1/2}\times\left(\frac{E\omega_{12}}{q_{12}q_3}\right)^{1/2}d_{0m_{12}}{}^{j_{12}}(\theta_3)\delta_{\mu+\mu_3,m_{12}}\times\langle\omega_{12}{}^2,\mu,\mu_3 j_{12}m_{12}|\,T_J(s)\,|m\rangle. \quad (2.4)$$

The production amplitude for each angular momentum state J has now been decomposed into a sum of contributions arising from the production of a dipion system of mass ω_{12}, angular momentum j_{12}, Z component m_{12}. Alternative decompositions based on $(\pi_1 N)\pi_2$ and $(\pi_2 N)\pi_1$ can also be made. The formulas are slightly more complicated because of the need for transformations on the nucleon spin. Wick[7] has given formulas for recoupling coefficients $\langle(12)3|1(23)\rangle$. This does not concern us in the present discussion because of our nonrelativistic spin approximation.

A further step in the fully relativistic treatment is the decomposition into eigenstates of orbital angular momentum.[12] This again we do not need to develop.

III. ISOBAR MODEL FOR PRODUCTION PROCESSES

In this section, we briefly review the theoretical basis for the isobar model[13–18] in order to see where we might expect our detailed model to fail.

Ideally, in order to use phenomenology, one would like a formalism that embodied unitarity and a limited amount of analyticity such as does the inverse K matrix for multichannel two-body processes. Even for the two-body case, this approach has limitations, where as is common the practically accessible reactions are all initiated from one channel. The position for the study of $2\to 3$ is more complicated. In order to apply unitarity, one has to discuss the processes $3\to 3$ [see Fig. 4(a)]. These contain, firstly, disconnected parts corresponding to two-body final-state interactions. Such contributions can in principle be determined from independent experiments at lower energies. There are in addition connected parts which cannot be learned from experiments. The isobar model arises from a simple approximate treatment of the disconnected parts (final-state interactions) and their effects; one constructs $2\to 3$ and $3\to 3$ amplitudes as if all final-state interactions comprised narrow resonances.

Firstly, one assumes that the production amplitude T (for a given J^P state) is expressible as a sum of three terms T_α classified according to which pair of particles interacts last.[19]

The singularity structure of production amplitudes is much more complicated than that of two-body scattering because there can be simultaneous discontinuities in s, ω_1, ω_2, and ω_3 (see, for example, Ref. 20). In the isobar model, the amplitudes are constructed to have only the simplest singularities. Precisely, T_α is taken to have the singularities which it would have if only the pair α underwent final-state interactions. Complex singularities arising from, for example, triangle graphs[21] are ignored.

In the case where the final-state interaction between the pair α is a narrow resonance, one pictures the process described by T_α as the production of the resonance followed by its decay. Thus one writes

$$T_\alpha=G(s,m_r)\frac{\sqrt{\Gamma}}{m_r-\omega_\alpha-i\Gamma/2}, \quad (3.1)$$

where G is the production amplitude for a particle of mass m_r, width Γ (the above formula is for an S-wave resonance). In the isobar model, this form is generalized and one takes

$$T_\alpha=G(s,\omega_\alpha)h(\omega_\alpha), \quad (3.2)$$

where

$$h(\omega_\alpha)=(\omega_\alpha/q_\alpha)e^{i\delta_\alpha}\sin\delta_\alpha, \quad (3.3)$$

with $\delta_\alpha(\omega_\alpha)$ the phase of the final-state interaction and where G contains no singularities in the variable ω_α in the physical region. Residual dependence of G on ω_α is commonly assumed to be simple and mainly kinematic[3,4]; for example, if the isobar is produced in an orbital state L, one inserts a factor $q_\alpha{}^L$, where q_α is the relative momentum of the α isobar and the third recoiling particle. A range parameter can also be introduced as a phenomenological form factor so that the above factor becomes $[q_\alpha/(1+Kq_\alpha{}^2)^{1/2}]^L$. If the isobar in question, formed, say of final particles i and j, decays into a state of orbital angular momentum l_{ij} with c.m. momentum q_{ij}, one inserts a further factor $q_{ij}{}^{-l_{ij}}$. This is to allow for the fact that the production amplitude contains only one isobar-ij vertex while the ij elastic amplitude contains two such. The effect of these assumptions is that for a reasonably narrow resonance the dependence of the cross section on ω_α is predominantly given by $\sin^2\delta_\alpha$.

[12] A. J. MacFarlane, Rev. Mod. Phys. **34**, 41 (1962).
[13] K. M. Watson, Phys. Rev. **88**, 1163 (1952); **95**, 228 (1954).
[14] L. F. Cook and B. W. Lee, Phys. Rev. **127**, 283 (1962).
[15] J. S. Ball, W. R. Frazer, and M. Nauenberg, Phys. Rev. **128**, 478 (1962).
[16] S. Mandelstam, J. E. Paton, R. F. Peierls, and A. Q. Sarker, Ann. Phys. (N. Y.) **18**, 198 (1962).
[17] G. N. Fleming, Phys. Rev. **135**, B551 (1964).
[18] D. Z. Freedman, C. Lovelace, and J. M. Namyslowski, Nuovo Cimento **43A**, 258 (1966).
[19] Fadeev has discussed the scattering processes $3\to 3$ for nonrelativistic systems governed by the successive action of two-body potentials between pairs: L. D. Fadeev, "Mathematical problems of the Quantum Theory of Scattering for a Three-Particle System" (English transl.: H. M. Stationery Office, Harwell, 1964). $T=\sum T_\alpha$ follows rigorously for this case. For production processes, $2\to 3$, there will be Born terms which cannot be classified as belonging to one of the T_α.
[20] S. Mandelstam, Phys. Rev. **140**, B375 (1965).
[21] I. J. R. Aitchison, Phys. Rev. **133**, B1257 (1964); C. Kacser, Phys. Letters **12**, 269 (1964).

The production amplitude $G(s,\omega_\alpha)$ will of course contain discontinuities as a function of the variable s. We will speak of the resulting phase as the *production phase* $\Phi_\alpha(s)$ and the phase $\delta_\alpha(\omega_\alpha)$ as the *decay phase*. The total phase of the T component of the production amplitude is then $\Phi_\alpha(s)+\delta_\alpha(\omega_\alpha)$, this being a special property of the model.

The form (3.2) embodies the Watson final-state theorem.[13] If the rescattering of the α pair were the only final-state interaction, it can be shown[14] that $2\to 3$ unitarity demands that the phase be δ_α, and more precisely that

$$T(s,\omega_\alpha{}^+)=e^{2i\delta_\alpha}T(s,\omega_\alpha{}^-)\,, \tag{3.4}$$

where $\omega_\alpha{}^\pm$ denote values of the partial energy ω_α above and below its cut. It then follows that the quantity $D(\omega_\alpha)\ T(s,\omega_\alpha)$ [where $h(\omega_\alpha)=N/D$] has no right-hand cut in ω_α. If the product DT is assumed not to depend too strongly on ω_α and if we make a similar assumption for the elastic N function, the Watson form is justified. One can imagine many circumstances where these assumptions are unjustified, especially where the final-state phase shift is slowly varying. Only attractive final-state interactions are taken into account.

In order to discuss unitarity in the more general situation where all the pairs of final particles can interact, it is necessary to complete the model so as to include the connected $3\to 3$ amplitudes. This is done by writing diagrams with isobar-particle vertices at both ends in the obvious way as shown in Fig. 4(b). It is then easy to show[16] that the isobar model satisfies $3\to 3$ unitarity provided all overlap contributions can be neglected [i.e., important contributions to three-body unitarity come only from terms $T_\alpha{}^\dagger T_\alpha$ and not from $T_\beta{}^\dagger T_\alpha$ (see diagrams in Ref. 16).]

The key assumptions are therefore: (1) The three-body production amplitude is approximately expressible as a sum of isobar production amplitudes. (2) There is approximate over-all orthogonality of contributions from isobars formed from different pairs. This implies that the phase dependence on ω_α has the form $e^{i\delta_\alpha}$. (One only assumes that the separate isobar contributions are approximately orthogonal when integrated over the Dalitz plot. They can, of course, interfere locally.) (3) One can apply the narrow-resonance approximation to give the other dependence on ω_α—the $\sin\delta_\alpha$ and kinematic factors.

Wright[22] has discussed the question of eigenstates for 3-body systems. The diagonalization of the T matrix is of course only to be applied to T_c for $3\to 3$. Applying the method to the isobar model, one can set up for example a one-level resonance formula with resonant contributions to the amplitudes of the form

$$\begin{aligned} T_{22}&=\frac{\frac{1}{2}\Gamma_0}{E_r-E-i\Gamma/2}\,,\\ T_{23}&=\sum_\alpha \frac{(\Gamma_0\Gamma_\alpha/4)^{1/2}}{E_r-E-i\Gamma/2}h_\alpha(\omega_\alpha)\,,\\ T_{33}{}^c&=\sum_{\alpha\beta} \frac{(\Gamma_\alpha\Gamma_\beta/4)^{1/2}}{E_r-E-i\Gamma/2}h_\alpha(\omega_\alpha)h_\beta(\omega_\beta)\,. \end{aligned} \tag{3.5}$$

If the final-state interactions do not overlap, this satisfies two- and three-body unitarity with real Γ_0, Γ. We will, therefore, expect for situations dominated by a one-level resonance that the production phase is equal to the elastic phase. In applications, we may expect to be beset by the usual complications of background and contributions from other eigenchannels.

Collecting together our assumptions, we have the following model. The production amplitude in a given J^P state is expressed as a sum of isobar contributions. These will arise from attractive final-state interactions among the three final-state pairs and each final-state pair will in general interact attractively in several two-particle angular momentum eigenstates. Formulas are conveniently expressed in terms of the double angular momentum decomposition [Eq. (2.4)]. We assume amplitudes to have been further decomposed into eigenstates of orbital angular momentum through Clebsch-Gordan transformations. Then our assumed form for an individual contribution to the production amplitude, say for the production of a particular (12) isobar, is [cf. Ref. 4]

$$t_J{}^{P(a)}\equiv\langle\omega_{12}{}^2 j_{12}l_{12}L_3|\,T_J(s)\,|\rangle=(q_{12}q_3)^{1/2}Be^{i\Phi} \times\frac{e^{i\delta_{12}}\sin\delta_{12}}{q_{12}}q_3{}^{L_3}\frac{(1+Kq_3{}^2)^{-L_3/2}}{q_{12}{}^{l_{12}}}\,. \tag{3.6}$$

Here the parameters B and Φ are functions of s only, l_{12} is the orbital angular momentum for the (12) subsystem, j_{12} its total angular momentum, and L_3 the orbital angular momentum of the relative motion of particle 3 and the (12) c.m. system. The factor $(q_{12}q_3)^{1/2}$ cancels the factor in Eq. (2.4) arising from our normalization. One could also add a factor $\omega_{12}{}^{-1/2}$. Whether one does so or not seems arbitrary and following Ref. (4) we have not done so. Likewise it is arbitrary to include a form factor as a function of q_3 but not of q_{12}. Such questions are not too important when the isobar comprises a narrow resonance. In the contrary case, all the factors expressing dependence on q_{12} are dubious. In the present application, $(\pi\pi)$ isobars are discussed which do not resonate at all in the range of phase space considered, so that use of the isobar formulas represents a considerable extrapolation.

Considerations in applying the model are as follows: (1) One chooses the lowest possible state of orbital

[22] J. A. Wright, Phys. Rev. **137**, B137 (1965).

TABLE I. Selection of parameters which have been inferred for the $I=0$ S-wave $\pi\pi$ phase shift.

Method	Result	Reference
πN partial-wave analysis	$a_0 \equiv (\omega/q)\cot\delta_0^0 = 1.3$ with δ_0^0 rising to a maximum of 30° at $T_\pi \sim 100$ MeV.	a
Analysis of πN backward dispersion relation (non-spin-flip) by fitting procedure	Fits with δ_0^0 resonance strongly preferred. Specially favored solutions of the type (a) a_0 positive $\sim 0.7\ \mu^{-1}$ with resonance at mass $\sim 430 \pm 70$ MeV, width 400_{-150}^{+400} MeV; (b) a_0 negative, δ_0^0 passing through 0° near 350 MeV, resonance at 680 ± 85 MeV, width 750 ± 50 MeV.	b
Analysis of peripheral single-pion production at high energies	Some results are as follows: (1) The analysis of Wolf gives δ_0^0 resonance position ~ 740 MeV, width 90 MeV.	c
	(2) Jacob and Selove estimates $\langle\delta_0^0\rangle \sim 35°$–$55°$ in 400–500 MeV mass interval.	d
	(3) Walker *et al.*—slowly varying $\pi\pi$ $I=0$, $I=2$ phase shifts. Preferred set has resonance at 850–950 MeV.	e
	(4) Clegg favors δ_0^0 slowly varying and $\sim 90°$ around 850–950 MeV.	f
K_{e4} decays-(preliminary results)	$\langle\delta_0^0 - \delta_1^1\rangle = +32° \pm 12°$. Result is average over the dipion mass spectrum which peaks to the lower mass values ~ 330 MeV.	g
Theory of decay branching ratios of η, etc.	"σ hypothesis" of Brown and Singer. $M_\sigma \sim 400$ MeV. $\Gamma_\sigma \sim 100$ MeV.	h
Current algebra and PCAC	Weinberg predicts $a_0 = 0.20\ \mu^{-1}$.	i
Current algebra $SU_2 \times SU_2$ for axial and vector charges as for the Adler-Weisberger relation	Adler consistency condition: This requires that the sum of weighted integrals of $\sin^2\delta_0^0$ and $\sin^2\delta_1^1$ exceed a certain value. Inserting conventional parameters for the ρ meson leaves a large contribution to come from low-energy $\pi\pi$ scattering, e.g., with scattering length parametrization $a_0 > 1.3$.	j

[a] J. Hamilton, P. Menotti, G. C. Oades, and L. L. J. Vick, Phys. Rev. **128**, 1881 (1962).
[b] C. Lovelace, R. M. Heinz, and A. Donnachie, Phys. Letters **22**, 332 (1966).
[c] G. Wolf, Phys. Letters **19**, 328 (1965).
[d] L. D. Jacobs and W. Selove, Phys. Rev. Letters **16**, 669 (1966).
[e] W. D. Walker, J. Carroll, A. Garfinkel, and B. Y. Oh, Phys. Rev. Letters **18**, 630 (1967).
[f] A. B. Clegg, Phys. Rev. **163**, 1664 (1967).
[g] Preliminary results form experiment by the Berkeley, U.C.L., Wisconsin collaboration presented by M. J. Esten at I.P.P.S. Conference at University College London, 1967.
[h] See review by L. M. Brown and H. Faier, in *Proceedings of Second Coral Gables Conference 1965* (W. H. Freeman and Co., San Francisco, 1965).
[i] S. Weinberg, Phys. Rev. Letters **17**, 616 (1966).
[j] See Ref. 25.

angular momentum L for the production of a given isobar in a given J^P state. In the present instance, only $L=0$ and 1 are considered. (2) In the present treatment, in contrast to some other analyses,[3,4] we do not trouble to construct orthogonal basis states. For example, we will discuss situations with P_{11} going simultaneously to the decay channels σN (S wave) and πN^* (P wave), states with nonvanishing overlap.

IV. SPECIFIC ISOBAR MODEL FOR πN-$\pi\pi N$ BELOW 700 MeV

As stated in the Introduction, our analysis will be confined to the partial waves $S_1(\frac{1}{2}^-)$, $P_1(\frac{1}{2}^+)$, $P_3(\frac{3}{2}^+)$ and $D_3(\frac{3}{2}^-)$ for $I=\frac{1}{2}$ and $\frac{3}{2}$. We consider the formation of the following isobars:

(a) $N^*(1236)$, πN, $I=\frac{3}{2}$, $J^P=\frac{3}{2}^+$;
(b) σ, $\pi\pi$, $I=0$, $J^P=0^+$;
(c) ρ, $\pi\pi$, $I=1$, $J^P=1^-$;
(d) N', πN, $I=\frac{1}{2}$, $J^P=\frac{1}{2}^-$.

The N^* is the classic candidate and needs no comment. The N' was introduced by OY[1,2] and we follow them in using this for production in the state P_{31}. The σ is also a popular candidate the only problem being the conflicting testimony on the detailed form of the $I=0$ S-wave $\pi\pi$ interaction. A selection of parameters which have been inferred is shown in Table I. The calculations reported in Sec. V are for a $\pi\pi$ phase δ_0^0 of the form

$$\delta_0^0 = \arctan\left[\frac{q}{\omega}\frac{[0.2+0.325(q^2/m_\pi^2)]}{1-0.1905(q^2/m_\pi^2)}\right]. \quad (4.1)$$

(In our notation q is q_{12}, ω is $\frac{1}{2}\omega_{12}$.) This form gives a scattering length $a_0=0.2\ \mu^{-1}$ with a broad resonance centered at 700 MeV. It was chosen by taking six different trial forms for δ_0^0 embodying different features which have been proposed (Table I) and seeing which looked best able to explain the shape of the $(\pi^+\pi^-)$mass spectrum at 558 MeV with P_{11} and D_{13} each decaying 50% to πN^* and 50% to σN. This discrimination is rather ill founded since we later conclude that D_{13} and P_{11} only account for $\frac{3}{4}$ of $\pi^+\pi^- n$ production at 558 MeV and that P_{11} decays significantly to ρN. One would like to re-open this question when better data becomes available. Meantime, the chosen form is not unreasonable.

The inclusion of the $I=1$, $J=1$ $\pi\pi$ final state was dictated by the phenomenology. There have been suggestions in other contexts that the very-low-energy tail of the ρ may be of importance—in the analysis of nucleon electromagnetic form factors[23] and in the study of 3π decays of η, τ, and τ'.[24] Very-low-energy $I=1$ contributions would be helpful in fitting the Adler consis-

[23] N. G. Antoniou and J. E. Bowcock, Phys. Rev. **159**, 1257 (1967).
[24] R. L. Schult and I. M. Barbour, Phys. Rev. **164**, 1791 (1967).

tency condition[25] without an unreasonably large $I=0$ component. Present calculations are based on a $\delta_1{}^1$ of the simple form

$$\delta_1{}^1=\arctan\left[\frac{q^3}{\omega}\frac{1.375}{1-0.1609q^2/\mu^2}\right] \tag{4.2}$$

corresponding to a resonance at 750 MeV, width 100 MeV.

Following Olsson[26], the δ_{33} phase shift for the N^* was taken to be of the form (with ω_{23} in GeV, q_{23} in GeV/c)

$$\delta_{33}=\arctan\left[\frac{17.06q_{23}{}^2}{(1.236-\omega_{23})(1+146.4q_{23}{}^2)}\right], \tag{4.3}$$

which gives a reasonable fit to the results from phase-shift analysis. The phase $\delta_1{}'$ for the N' was taken to be[1]

$$\delta_1{}'=\arctan(4.63q_{31}). \tag{4.4}$$

Note that the assumed forms for the $\pi\pi$ phases $\delta_0{}^0$ and $\delta_1{}^1$ correspond to broad resonances outside the region of phase space to be studied so that the terms σ and ρ are to be regarded in the present context as a shorthand for $\pi\pi$ quantum numbers.

In accord with our philosophy of preferring low orbital angular momenta, we confine the discussion of possible contributions to the partial-wave production amplitudes to the modes listed in Table II.

TABLE II. Isobar contributions to the partial-wave production amplitudes.

	πN^* (1) $\pi_1N_{23}{}^*$	πN^* (2) $\pi_2N_{13}{}^*$	σN (3)	ρN (4)	ρN (5)	$\pi N'$ (6) $\pi_1N_{23}{}'$	$\pi N'$ (7) $\pi_2N_{12}{}'$
S_1			P wave	S wave			
P_1	P wave		S wave	P wave		S wave	
P_3	P wave			P wave			
D_3	S wave		P wave	S wave			

The modes are labeled (1) to (7) as shown. The duplication of πN^* and $\pi N'$ labels arises from the two possible πN pairings. The extra label for ρN is used to distinguish the two possible couplings to the P_1 state, $j_{12}+L_3=0$ (mode 4) and $j_{12}+L_3=1$ (mode 5). The σN modes contribute only to the $I=\frac{1}{2}$ states. The termination of the list is arbitrary and other authors have used different subsets. For example, NRR[3] have considered D-wave πN^*.

We now list the required angular momentum projection operators. These are expressed as scalar functions of the Pauli spin matrices and the unit vectors defined in Sec. II.

$$\begin{aligned}
&S_1{}^{(3)}=\boldsymbol{\sigma}\cdot\hat{q}_3,\\
&S_1{}^{(4)}=\boldsymbol{\sigma}\cdot\hat{q}_{12},\\
&P_1{}^{(1)}=2(\boldsymbol{\sigma}\cdot\hat{q}_A)(\hat{q}_1\cdot\hat{q}_{23})-(\boldsymbol{\sigma}\cdot\hat{q}_{23})(\hat{q}_1\cdot\hat{q}_A)\\
&\qquad\qquad+(\boldsymbol{\sigma}\cdot\hat{q}_1)(\hat{q}_{23}\cdot\hat{q}_A)+i\hat{q}_A\cdot(\hat{q}_1\times\hat{q}_{23}),\\
&P_1{}^{(2)}=(\text{expression for } P_1{}^{(1)} \text{ with } 1\leftrightarrow 2),\\
&P_1{}^{(3)}=\boldsymbol{\sigma}\cdot\hat{q}_A,\\
&P_1{}^{(4)}=(\boldsymbol{\sigma}\cdot\hat{q}_A)(\hat{q}_{12}\cdot\hat{q}_3),\\
&P_1{}^{(5)}=i(\boldsymbol{\sigma}\cdot\hat{q}_3\times\hat{q}_{12})(\boldsymbol{\sigma}\cdot\hat{q}_A)\\
&\qquad=(\boldsymbol{\sigma}\cdot\hat{q}_3)(\hat{q}_A\cdot\hat{q}_{12})-(\boldsymbol{\sigma}\cdot\hat{q}_{12})(\hat{q}_A\cdot\hat{q}_3)\\
&\qquad\qquad+i\hat{q}_A\cdot(\hat{q}_3\times\hat{q}_{12}),\\
&P_1{}^{(6)}=P_1{}^{(7)}=P_1{}^{(3)},\\
&P_3{}^{(1)}=-\tfrac{1}{2}(\boldsymbol{\sigma}\cdot\hat{q}_A)(\hat{q}_1\cdot\hat{q}_{23})-\tfrac{1}{2}(\boldsymbol{\sigma}\cdot\hat{q}_{23})(\hat{q}_1\cdot\hat{q}_A)\\
&\qquad\qquad+2(\boldsymbol{\sigma}\cdot\hat{q}_1)(\hat{q}_{23}\cdot\hat{q}_A)-\tfrac{5}{2}i\hat{q}_A\cdot(\hat{q}_1\times\hat{q}_{23}),\\
&P_3{}^{(2)}=(\text{expression for } P_3{}^{(3)} \text{ with } 1\leftrightarrow 2),\\
&D_3{}^{(1)}=3(\boldsymbol{\sigma}\cdot\hat{q}_A)(\hat{q}_{23}\cdot\hat{q}_A)-\boldsymbol{\sigma}\cdot\hat{q}_{23},\\
&D_3{}^{(2)}=(\text{expression for } D_3{}^{(1)} \text{ with } 1\leftrightarrow 2),\\
&D_3{}^{(3)}=3(\sigma\cdot\hat{q}_A)(\hat{q}_3\cdot\hat{q}_A)-\boldsymbol{\sigma}\cdot\hat{q}_3,\\
&D_3{}^{(4)}=3(\boldsymbol{\sigma}\cdot\hat{q}_A)(\hat{q}_{12}\cdot\hat{q}_A)-\boldsymbol{\sigma}\cdot\hat{q}_{12}.
\end{aligned} \tag{4.5}$$

The derivation is straightforward. Helicity amplitudes may be derived by taking expectation values between the appropriate Pauli spinors. The formalism is exact for the $(\pi\pi)N$ contributions; for $\pi(\pi N)$ a small approximation is involved (see Appendix A). For production off unpolarized targets, this only affects interference terms in the cross section.

The total production amplitude is now expressible as a sum of contributions

$$T=T_{S_1}+T_{P_1}+T_{P_3}+T_{D_3}, \tag{4.6}$$

where for instance

$$T_{D_3}=\sum_{i=1}^{4}B_{D_{13}{}^{(i)}}e^{i\Phi_{D_{13}{}^{(i)}}}F_{D_3{}^{(i)}}D_3{}^{(i)}$$
$$+\text{similar contribution from } I=\tfrac{3}{2}. \tag{4.7}$$

Here the $B_{D_{13}{}^{(i)}}$ and $\Phi_{D_{13}{}^{(i)}}$ are parameters depending only on s as discussed in Sec. III, the $D_3{}^{(i)}$ are the angular momentum projection operators and the $F_{D_3{}^{(i)}}$ are the isobar production formulas. Examples are

$$F_{D_3{}^{(1)}}=(q_{23}q_1)^{1/2}\frac{e^{i\delta_{33}}\sin\delta_{33}}{q_{23}{}^2},\quad \delta_{33}=\delta_{33}(q_{23}{}^2), \tag{4.8}$$

$$F_{D_3{}^{(3)}}=(q_{12}q_3)^{1/2}\frac{e^{i\delta_0}\sin\delta_0}{q_{12}}$$
$$\times q_3(1+K_\sigma q_3{}^2)^{-1/2},\quad \delta_0=\delta_0(q_{12}{}^2). \tag{4.9}$$

Here K_σ is the range parameter for P-wave σ production, There are similar parameters K_ρ and K_{N^*} occurring

[25] S. L. Adler, Phys. Rev. **140**, B736 (1965).
[26] M. G. Olsson, Phys. Rev. Letters **14**, 118 (1965).

TABLE III. Sample of the overlap coefficents I_{ij} and J_{ij} [Eq. (4.13)]. The matrices plotted are I_{ij} (ordinary numerals) for $i \leqslant j$ and J_{ij} for (italicized numerals) $i > j$. Quantities are calculated with the parameters given in Sec. IV for $T_\pi = 558$ MeV.

S_1	σN	ρN					
	1.0	0.0					
	0.0	1.0					
P_1	$\pi_1 N^*$	$\pi_2 N^*$	σN	$(\rho N)_4$	$(\rho N)_5$	$\pi_1 N'$	$\pi_2 N'$
	1.0	0.135	−0.195	0.003	0.273	0.010	−0.035
	0.0	1.0	−0.198	0.007	−0.273	−0.037	0.007
	0.091	*0.093*	1.0	0.002	0.0	0.896	0.897
	−0.117	*0.116*	*0.003*	1.0	0.0	−0.026	0.029
	0.363	*−0.363*	*0.0*	*0.0*	1.0	0.0	0.0
	−0.027	*−0.012*	*−0.100*	*0.228*	*0.0*	1.0	0.891
	−0.013	*−0.023*	*−0.101*	*−0.229*	*0.0*	*0.0*	1.0
P_3	$\pi_1 N^*$	$\pi_2 N^*$					
	1.0	0.457					
	0.0	1.0					
D_3	$\pi_1 N^*$	$\pi_2 N^*$	σN	ρN			
	1.0	0.455	−0.347	−0.183			
	−0.487	1.0	−0.346	0.184			
	−0.397	*−0.397*	1.0	0.00			
	−0.441	*0.441*	*0.0*	1.0			

in $P_1^{(4)(5)}$ and $P_1^{(1)(2)}$ (also $P_3^{(1)(2)}$). In the calculations to be reported, these parameters were set to the common value[27]

$$K_\sigma = K_\rho = K_{N^*} = 8.163\ (\mathrm{GeV}/c)^{-2} = (350\ \mathrm{MeV}/c)^{-2}. \quad (4.10)$$

According to formula (2.1), the total production cross section is given by

$$\sigma = \frac{\pi^3}{16 E^3 q_A} \sum_{\text{spin av.}} \int d\omega_1\, d\omega_2\, d(\cos\Theta) d\Phi\, |T|^2. \quad (4.11)$$

Dalitz-plot distributions and mass spectra are obtained by omitting the appropriate integrations. Whenever we integrate over the production solid angle, contributions from different J^P state decouple. In particular, the partial-wave production cross sections have simple expressions as integrals over the Dalitz plot. We make use of averages over spin and the incoming direction $\hat{q}_A$ of the bilinear expressions in the angular momentum projection operators. For example,

$$\langle (P_1^{(1)})^2 \rangle = 1 + 3(\hat{q}_1 \cdot \hat{q}_{23})^2,\ \langle P_1^{(3)} \cdot P_1^{(4)} \rangle = \hat{q}_{12} \cdot \hat{q}_3. \quad (4.12)$$

The resulting total cross section takes the form

$$\sum_{i \leqslant j} B_{J^P(i)} B_{J^P(j)} [\cos(\Phi^{(i)} - \Phi^{(j)})\, I_{ij} + \sin(\Phi^{(i)} - \Phi^{(j)})\, J_{ij}]. \quad (4.13)$$

Similarly, for the Dalitz-plot density with suitable reinterpretation of J_{ij} and J_{ij}.

The $B^{(i)}$ are renormalized: $B^{(i)} = ZU^{(i)}$ with $\sum_i (U^{(i)})^2 = 1$. Z is chosen so that in the expression for the total cross section the $I_{ii} = 1$ and the total partial-wave cross section takes the value

$$\sigma_{\text{in}}(J^P) = (\pi/q_{AB^2})(J + \tfrac{1}{2})(1 - \eta_{J^P}{}^2). \quad (4.14)$$

Here η_{J^P} is the appropriate inelasticity parameter occurring in the πN elastic phase-shift analysis, if we assume that all the inelasticity goes to $\pi\pi N$ (see discussion in Sec. V). Hypotheses for the inelastic output of a given state are then specified by assigning the quantity η and the ratios $U^{(i)}$. Where a given hypothesis involves two amplitudes, e.g., $P_1 \to \pi N^*$ with π_1 ($N_{23}{}^*$) and π_2 ($N_{31}{}^*$), we group these appropriately. In this way, we are able to construct amplitudes with say $P_1 \to \pi N^*$ 60% and $\to \sigma N$ 40%.

A computed set of values for the matrices I_{ij}, J_{ij}, the overlap coefficients as we may term them, is listed in Table III. They are computed for the parameters listed above and for $T_\pi(\text{lab}) = 558$ MeV. It will be noted that a number of the overlap coefficients are small which lends support to that aspect of the isobar model.

In order to take account of different charge final states we require the products of Clebsch-Gordan coefficients by which the amplitudes previously written down must be multiplied. These are listed in Table IV, which is an extension of that given by OY.[1] As stated earlier, we adopt the convention that particle 1 is the pion of larger charge, particle 2 the other pion, and particle 3 the nucleon.

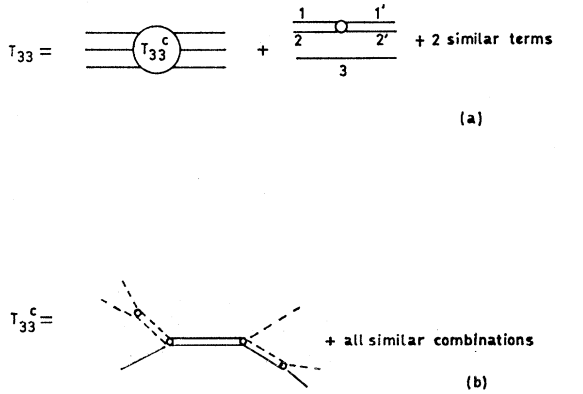

FIG. 4. (a) General structure of $3 \to 3$ amplitudes. (b) Schematic of the isobar model for the connected part.

[27] Cf. A. N. Mitra and M. Ross, Phys. Rev. **158**, 1630 (1967).

TABLE IV. Isotopic-spin factors in isobar production amplitudes.

Reaction	σN	ρN $(I=\frac{3}{2})$	ρN $(I=\frac{1}{2})$	$\pi_1 N^*$ $(I=\frac{3}{2})$	$\pi_1 N^*$ $(I=\frac{1}{2})$	$\pi_2 N^*$ $(I=\frac{3}{2})$	$\pi_2 N^*$ $(I=\frac{1}{2})$	$\pi_1 N'$ $(I=\frac{3}{2})$	$\pi_2 N'$ $(I=\frac{3}{2})$
I: $\pi^+p\to\pi^+\pi^0p$	0	1	0	$-2/\sqrt{15}$	0	$3/\sqrt{15}$	0	$-1/\sqrt{3}$	0
II: $\pi^+p\to\pi^+\pi^+n$	0	0	0	$-1/\sqrt{15}$	0	$-1/\sqrt{15}$	0	$1/\sqrt{3}$	$1/\sqrt{3}$
III: $\pi^-p\to\pi^0\pi^-p$	0	1/3	2/3	$-1/3\sqrt{15}$	$2/3\sqrt{6}$	$4/3\sqrt{15}$	$-2/3\sqrt{6}$	$-2/3\sqrt{3}$	$-1/3\sqrt{3}$
IV: $\pi^-p\to\pi^+\pi^-n$	$-2/3$	$\sqrt{2}/3$	$-\sqrt{2}/3$	$-2/\sqrt{30}$	$-1/\sqrt{3}$	$4/3\sqrt{30}$	$-1/3\sqrt{3}$	0	$2/3\sqrt{6}$
V: $\pi^-p\to\pi^0\pi^0n$	$\sqrt{2}/3$	0	0	$-1/3\sqrt{15}$	$2/3\sqrt{6}$	$-1/3\sqrt{15}$	$2/3\sqrt{6}$	$1/3\sqrt{3}$	$1/3\sqrt{3}$

A computer program TRIBOD was written for the IBM 360 computer at the Rutherford Laboratory. The input to the program comprises the chosen form for the final-state phase shifts and the form-factor parameters; also the inelasticity, production phases, and hypothesis parameters $U^{(i)}$ for each partial wave. The program then produces charge branching ratios and for whatever charge channels are of interest, two-particle mass spectra. This is done by straightforward quadrature after the renormalization described. There is also a provision to generate the Dalitz-plot distribution for selected ranges of the production angles Θ_i and also the over-all Dalitz plot. These are computed by a Monte Carlo technique so that the averages over spin and azimuthal angle which occur in the many cross terms from isobar contributions to different spin parity states need not be programmed but are computed. This considerably simplifies the expressions appearing in the program and facilitates checking. Over-all production angular distributions $d\sigma/d\cos\Theta_i$ are also generated. Commonly, four ranges of $\cos\Theta_i$ were used $[\cos\Theta_i=-1(\frac{1}{2})1]$ in order to reveal up to cubic terms in $\cos\Theta_i$. Checking for cases with known distribution, it was found that 60 Monte Carlo events per angular interval gave fairly adequate results with reasonable computing times.

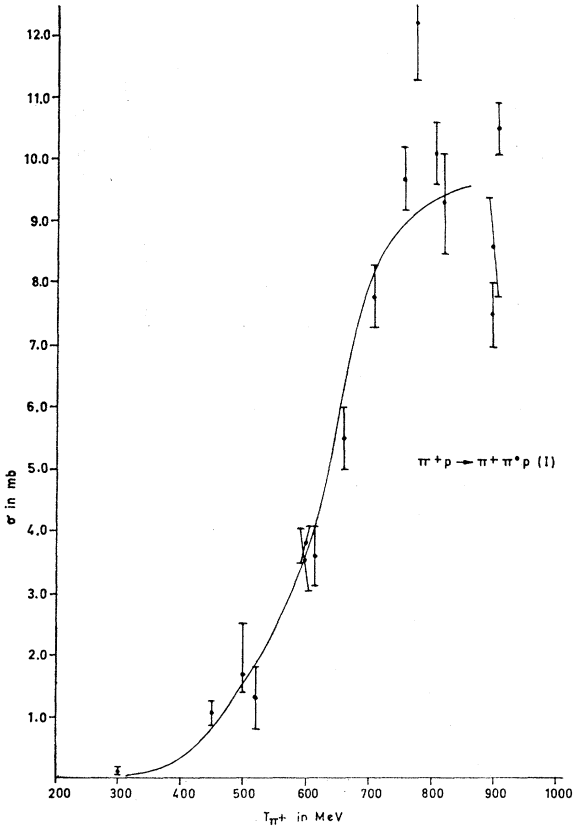

FIG. 5. Cross section for reaction I: $\pi^+p\to\pi^+\pi^0p$. The solid curve is the fit of OY.

V. DISCUSSION OF THE DATA

Essentially all the published data on single-pion production processes below 1 GeV have been reviewed by OY.[1,2] They achieve quite a comprehensive fit to the data in terms of a simple isobar model. The object of the present analysis is to suggest improvements in the light of current knowledge and to emphasize what should be looked for in the new higher statistics experiments which are under way. We shall put more emphasis than OY on the information from recent phase-shift analyses of elastic πN scattering (EPS).[28–30] For production data, we draw principally on the π^-p experiments at 558,[31] 604,[32] and 646 MeV.[33]

There is information on the five processes

$$\pi^+p\to\pi^+\pi^0p, \quad \text{(I)}$$
$$\pi^+p\to\pi^+\pi^+n, \quad \text{(II)}$$
$$\pi^-p\to\pi^0\pi^-p, \quad \text{(III)}$$
$$\pi^-p\to\pi^+\pi^-n, \quad \text{(IV)}$$
$$\pi^-p\to\pi^0\pi^0n. \quad \text{(V)}$$

The convention has been to present the data in the form of certain averages: total production cross section, over-all Dalitz plot (i.e., integrated over production angles), and projections of the plot (mass plots); finally, production angular distributions averaged over the Dalitz

[28] B. H. Bransden, P. J. O'Donnell, and R. G. Moorhouse, Phys. Rev. **139**, B1566 (1965).
[29] P. Bareyre, C. Bricman, A. V. Stirling, and G. Villet, Phys. Letters **18**, 342 (1965).
[30] P. Auvil, C. Lovelace, A. Donnachie, and A. T. Lea, Phys. Letters **12**, 76 (1964); **19**, 148 (1965); A. Donnachie, R. G. Kirsopp, A. T. Lea, and C. Lovelace (DKLL) (to be published). Results are summarized in Ref. 43.
[31] R. A. Burnstein *et al.*, Phys. Rev. **137**, B1044 (1965).
[32] C. N. Vittitoe *et al.*, Phys. Rev. **135**, B232 (1964).
[33] J. D. Oliver, I. Nadelhaft, and G. B. Yodh, Phys. Rev. **147**, 932 (1966).

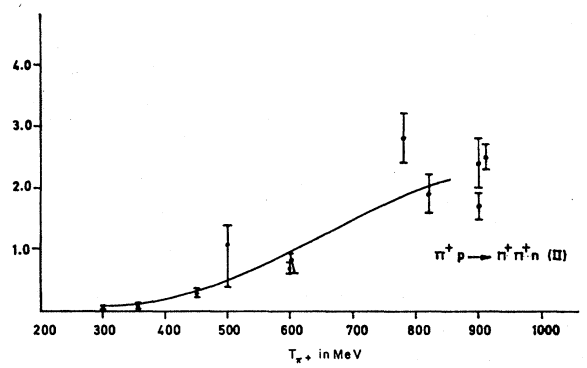

FIG. 6. Cross section for reaction II: $\pi^+ p \rightarrow \pi^+\pi^+ n$. The solid curve is the fit of OY.

plot. A summary of total production cross sections to the different charge channels taken from the compilation in Ref. 1 is presented in Figs. 5–9. Production angular distributions $d\sigma/d\cos\Theta_i$ for reactions III and IV from the experiments[31–32] at 558, 604, and 646 MeV are shown in Figs. 10–12, The mass spectra from the experiment at 558 MeV are shown in Fig. 13.

The OY model attributes production predominantly to the following partial waves and decay modes

$$I=\tfrac{3}{2}: D_{33}\ (S\text{-wave}\ \pi N^*)$$
$$P_{31}\ (P\text{-wave}\ \pi N^*\ \text{and}\ S\text{-wave}\ \pi N')$$
$$I=\tfrac{1}{2}: D_{13}\ (S\text{-wave}\ \pi N^*)$$
$$P_{11}\ (S\text{-wave}\ \pi N').$$

It attributes no energy dependence to the isobar production amplitudes $G(s,\omega_\alpha)$ except, where relevant, for kinematic threshold factors and an energy-dependent phase for D_{13} production. (OY have also to make certain adjustments, to comply with unitarity at the higher end of the energy range which they cover). They fit a wide range of production data with very few parameters. A key point in their fit is to reproduce the observed charge branching ratios between the total production cross sections for processes III, IV, V (Figs. 7–9). This is achieved through an energy-dependent interference between D_{13} and D_{33} production which is attributed to a rising phase Φ_1 of the D_{13} production amplitude. This is taken to pass through 90° at $T_\pi = 500$ MeV and causes a marked increase in σ(III) and decrease in σ(IV) over that which would be obtained if Φ_1 were 0°. At the same time quite a reasonable fit is achieved to the $\pi^+\pi^- n$ production angular distributions at 558 MeV, Fig. 10, which show strong quadratic effects. The OY analysis can thus be said to give independent confirmation on the existence of the D_{13} resonance.

Successful fits are also achieved to two-body mass spectra (e.g., Fig. 13) except for $\pi^+\pi^-$ from reaction IV. The excess of events with values of $\pi^+\pi^-$ mass at the upper end of phase space, the so called "Kirz anomaly," is well known and commonly attributed to $\pi\pi$ final-state interactions in the $I=0$, $J=0$ state. Since the effect is especially marked at low energies, it seems likely that the P_{11} state has an important $N\sigma$ decay channel. There may also at low energies be triangle

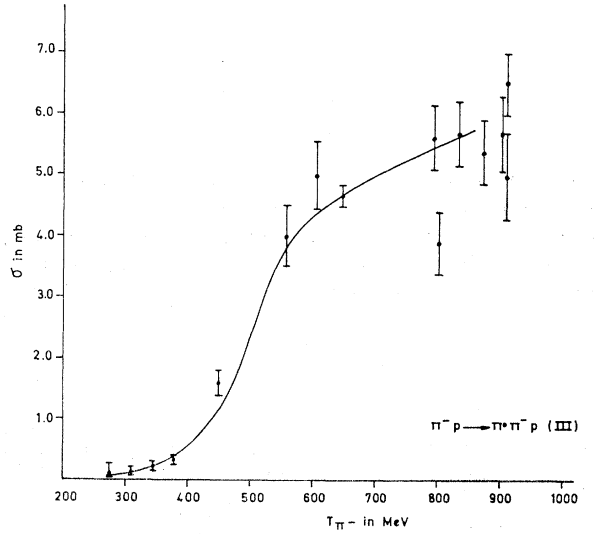

FIG. 7. Cross section for reaction III: $\pi^- p \rightarrow \pi^0\pi^- p$. The solid curve is the fit of OY.

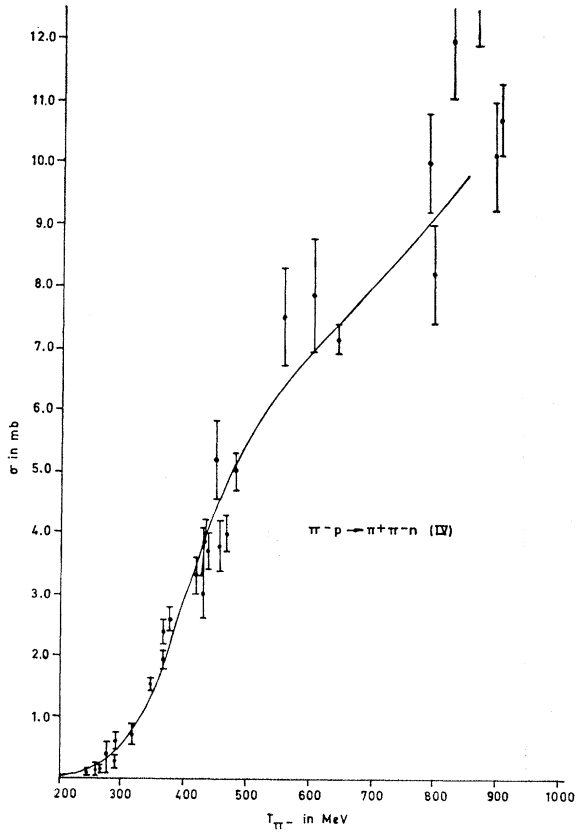

FIG. 8. Cross section for reaction IV: $\pi^- p \rightarrow \pi^+\pi^- n$. The solid curve is the fit of OY.

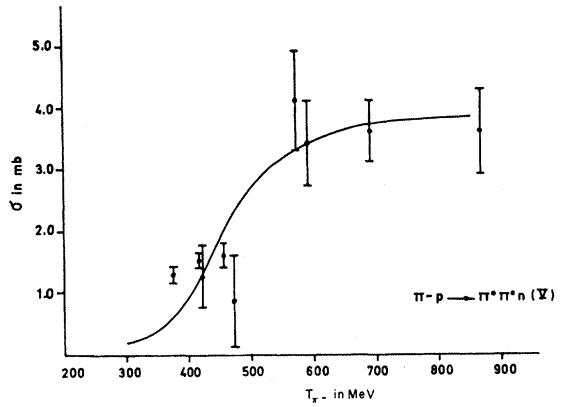

FIG. 9. Cross section for reaction V: $\pi^- p \to \pi^0\pi^0 n$. The solid curve is the fit of OY.

effects,[34] although doubt has been cast on existing calculations.[35]

Among the striking successes of OY with regard to spectra is the fitting of the observed peaking towards high mass of the $\pi^-\pi^0$ mass spectrum, Fig. 13(c), which is explained through an interference between the two N^* bands from D_{13}.

Problems with the OY analysis in addition to the Kirz anomaly are as follows:

(1) They do not reproduce the production angular distribution for reaction III ($\pi^-\pi^0 p$) at 558 MeV.[31] Just as for reaction IV, they predict substantial quadratic terms which the data do not show (see Fig. 10). Neither do they at 604 MeV[32] (Fig. 11). Taken together, these data suggest essentially isotropic production. At 646 MeV,[33] some deviation from isotropy is seen (Fig. 12) but still not in agreement with the model.

(2) The assumed partial-wave inelastic cross sections for D_{13} and P_{11} are in gross disagreement with the EPS results (see Fig. 14). Too much is attributed to D_{13} especially at low energies and too little to P_{11}.

We are thus led to attempt a fresh apportionment of the production cross section. The information from EPS on total production cross sections in various partial-wave channels is summarized in Figs. 15 and 16. We employ recent analyses published by three independent groups.[28–30] For $I=\frac{1}{2}$, the essential features are (i) large production in P_{11}—already marked at $T_\pi=300$ MeV and peaking somewhere between 400 and 500 MeV; (ii) strong production of the D_{13} resonance rising rapidly from $T_\pi=400$ MeV and peaking at around 600 MeV; (iii) considerable inelastic cross sections in S_{11}, certainly above the η threshold at 556

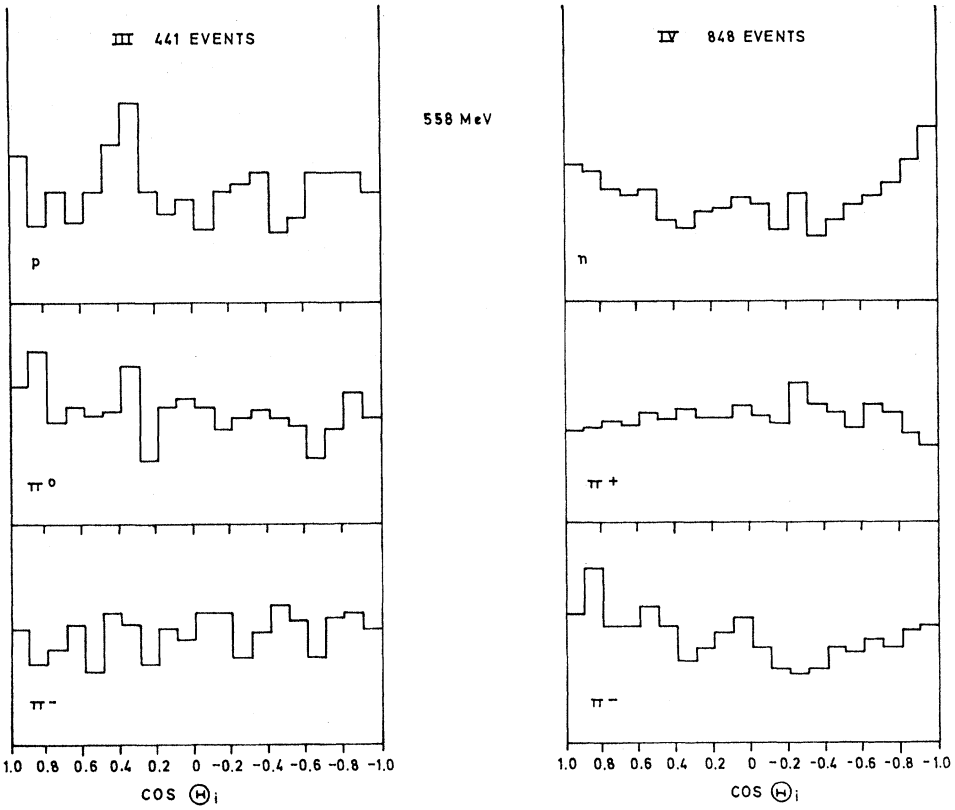

FIG. 10. Production angular distributions for reactions III and IV at 558 MeV (from Ref. 31).

[34] V. V. Anisovitch and L. G. Dakhno, Phys. Letters **10**, 221 (1964); also Zh. Eksperim. i Teor. Fiz. **46**, 1307 (1964) [English transl.: Soviet Phys.—JETP **19**, 886 (1964)].
[35] I. J. R. Aitchison, Nuovo Cimento **51A**, 272 (1967).

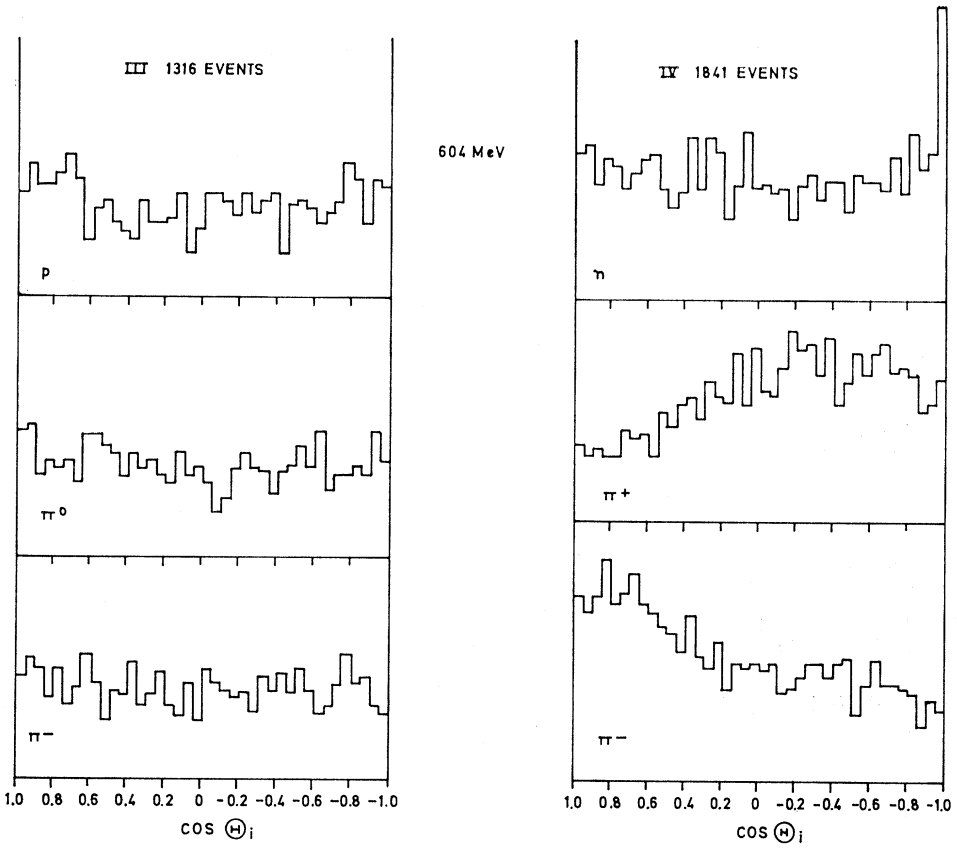

FIG. 11. Production angular distributions for reactions III and IV at 604MeV (from Ref. 32).

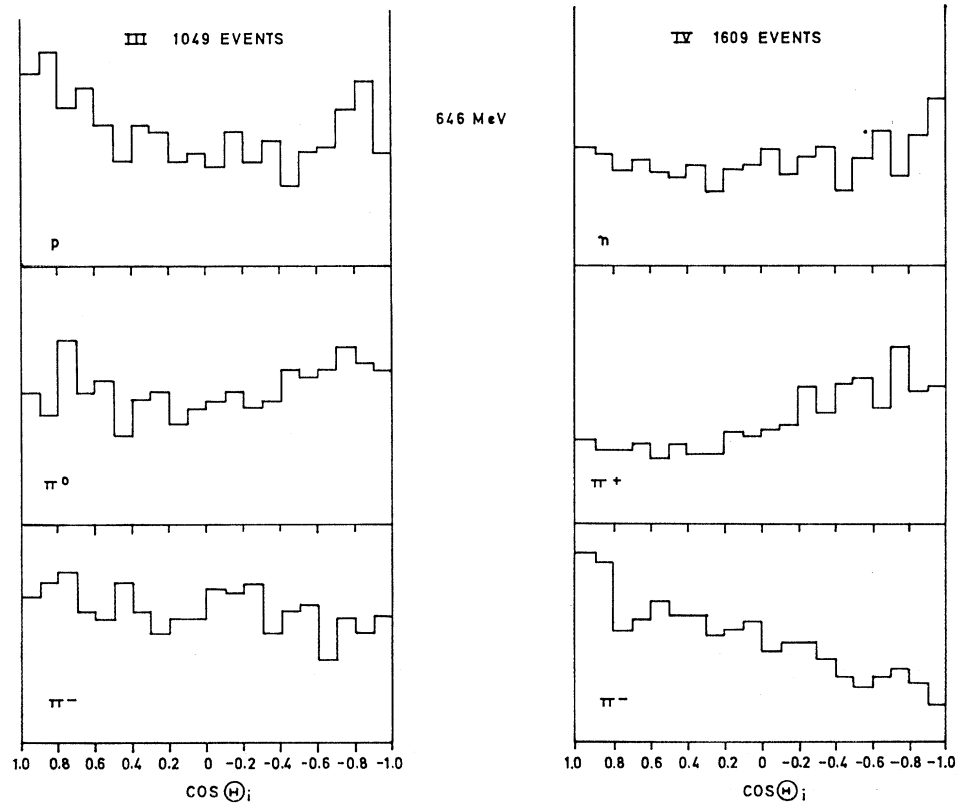

FIG. 12. Production angular distributions for reactions III and IV at 646 MeV (from Ref. 33).

MeV—possibly with a significant amount below; (iv) possibly quite a large P_{13} constribution.

For $I=\frac{3}{2}$, there is a good deal less unanimity.[36] It seems possible that the low-energy production, $T_\pi \lesssim 600$ MeV, is correctly described by OY as predominantly D_{33} supplemented by P_{31}. At any rate, we will follow this for the purpose of analyzing the $I=\frac{1}{2}$ contributions.

The elastic analyses can, of course, give us at most total inelastic cross sections σ_{J^P} ($\pi N \to$ all inelastic channels). However, experiment shows that the cross section for producing a final state with three or more pions, also that for associated production of strange particles, is in general small. We are thus safe in identifying the cross sections of Figs. 15 and 16 with those for the process $\sigma(\pi N \to \pi\pi N)$. An exception is furnished by the channel S_{11} where an important, possibly the predominant inelastic process is $\pi N \to \eta N$.[37,38] A rough consistency check is afforded by comparing the total inelastic cross sections for $\pi^- p$ and $\pi^+ p$ deduced from the elastic phase shifts with production data, see Figs. 17 and 18. The points are computed from EPS parameters and the curves are interpolations of the production data Figs. 5–9. The agreement is reasonably except for the case of $\pi^- p$ from $T_\pi = 550$ to about 700 MeV, the region where η production is observed.

One would like to determine the decay channels for the different partial waves but it does not seem possible to do this uniquely with the existing data. Certain constraints can however be inferred. The first evidence which may be used is that of the over-all charge branching ratios $\sigma(\mathrm{I}):\sigma(\mathrm{II}):\sigma(\mathrm{III}):\sigma(\mathrm{IV}):\sigma(\mathrm{V})$. The data on these quantities which have been compiled by OY are shown in Figs. 5–9. Using this information, one can make an isotopic-spin analysis of pion production. Production amplitudes can be characterized by the total isospin I and for instance the isospin I_π of the pion pair in the final state. We write $A_{I_\pi}{}^I$ for the amplitudes and there are just four of them—$A_1{}^{3/2}$, $A_2{}^{3/2}$, $A_0{}^{1/2}$, $A_1{}^{1/2}$. From Bose statistics, only the pairs $A_0{}^{1/2}$, $A_2{}^{3/2}$ and $A_1{}^{3/2}$, $A_1{}^{1/2}$ can interfere. The cross sections $\sigma(\mathrm{I})$ to $\sigma(\mathrm{V})$ can be written down using standard Clebsch-Gordan formulas:

$$
\begin{aligned}
\sigma(\mathrm{I}) &= \sigma(1^{3/2}) + \tfrac{1}{5}\sigma(2^{3/2}),\\
\sigma(\mathrm{II}) &= \tfrac{4}{5}\sigma(2^{3/2}),\\
\sigma(\mathrm{III}) &= \tfrac{1}{9}\sigma(1^{3/2}) + (4/9)\sigma(1^{1/2}) + (1/5)\sigma(2^{3/2})\\
&\quad + (4/9)[\sigma(1^{1/2})\sigma(1^{3/2})]^{1/2} X^{(-)},\\
\sigma(\mathrm{IV}) &= (2/9)\sigma(1^{3/2}) + (2/9)\sigma(1^{1/2}) - (4/9)\\
&\quad \times [\sigma(1^{1/2})\sigma(1^{3/2})]^{1/2} X^{(-)} + (4/9)\sigma(0^{1/2})\\
&\quad + (2/45)\sigma(2^{3/2}) + (4/9)(\sqrt{\tfrac{2}{5}})\\
&\quad \times [\sigma(0^{1/2})\sigma(2^{3/2})]^{1/2} X^{(+)},\\
\sigma(\mathrm{V}) &= (2/9)\sigma(0^{1/2}) + (4/45)\sigma(2^{3/2}) - (4/9)(\sqrt{\tfrac{2}{5}})\\
&\quad \times [\sigma(0^{1/2})\sigma(2^{3/2})]^{1/2} X^{(+)}.
\end{aligned}
\tag{5.1}
$$

The $\sigma(I_\pi{}^I) = \langle | A_{I_\pi}{}^I | ^2 \rangle$ and the $X^{(+)}$, $X^{(-)}$ are overlap coefficients which have to have modulus less than or equal to one. $X^{(+)}$ or $X^{(-)}$ equal to unity would imply that the interfering amplitude had exactly the same dependence on the kinematic variables and were in phase. (We have remarked how OY use a phase difference between D_{13} and D_{33} to achieve a charge-branching ratio varying with energy.) The first two equations give $\sigma(1^{3/2})$ and $\sigma(2^{3/2})$ uniquely. The remaining three cross sections are expressed in terms of four parameters. Of these, we can deduce the sum $\sigma(1^{1/2})+\sigma(0^{1/2})$ from the sum $\sigma(\mathrm{III})+\sigma(\mathrm{IV})+\sigma(\mathrm{V})$ and the $I=\frac{3}{2}$ data since the interferences cancel in the sum. To make further progress, we use the constraints $|X^{(\pm)}| \leqslant 1$. If one makes a plot of $\sigma(1^{1/2})$ against $\sigma(0^{1/2})$, the information on sums of cross sections constrains the allowed region to a line and the inequalities on the X's to a sector, in some cases quite a short sector. In this way, one constructs a rough plot of the ratio $R=\sigma(1^{1/2})/\sigma(0^{1/2})$ as a function of energy. This is shown in Fig. 19 where the error bars correspond to the allowed sector lengths referred to above. The main result is that there is an upward trend of R with increasing energy. Fig. 20 is a sketch of the total $I=\frac{1}{2}$ contribution to production from $\pi^- p$ and probable partial-wave contributions to it.

We shall discuss various hypotheses for the decay channels from the J^P production channels known to be relevant. The hypotheses considered will involve appropriate orbital states of πN^*, σN, ρN, and $\pi N'$. It is worth noting the values of the ratio $R=\sigma(1^{1/2})/\sigma(0^{1/2})$ for these. Thus, for πN^*, $R=\frac{1}{2}$ [assuming no interference between $(\pi_1 N)\pi_2$ and $(\pi_2 N)\pi_1$, a reasonable first approximation]; for $\pi N'$ (same no interference assumption) $R=2/1$; with the opposite assumption of total interference between $(\pi_1 N)\pi_2$ and $(\pi_2 N)\pi_2$, which is more reasonable for P_{11} especially at low energies, $R=0$. For σN and ρN, R is of course, respectively, 0 and ∞.

We have listed in the previous section the decay hypotheses which will be considered. For example, $P_{11} \to$ S-wave σN, P-wave πN^*, and P-wave ρN. (We do not use the $\pi N'$ hypothesis; it overlaps considerably with σN so that its use would lead to redundancy.) P_{11} is known to be the main inelastic channel at the lower energies and the ratio R seems to be tending to zero towards threshold. Therefore, it is plausible to assume that $P_{11} \to N\sigma$ S wave predominates at threshold. However, the admittedly rough analysis leading to Fig. 19 suggests that the ratio R is already significantly different from zero say $\sim\frac{1}{4}$ at $T_\pi = 450$ MeV. At this energy, P_{11} still predominates to a sufficient extent that we are led to assume $P_{11} \to$ other channels as well, for exam-

[36] Bransden *et al.*, (See Ref. 28) (BOM) have significant inelasticity in D_{35} and not in D_{33}. However, new phase-shift searches undertaken by B. H. Bransden, A. T. Davies, and R. G. Moorhouse indicate more inelasticity in D_{33} [R. G. Moorhouse (private communication)].

[37] References are given by A. T. Davies and R. G. Moorhouse, Rutherford Laboratory Report No. RPP/A8, 1966 (unpublished); and (to be published).

[38] F. Bulos *et al.*, Phys. Rev. Letters **13**, 486 (1964); W. B. Richards *et al.*, *ibid.* **16**, 1221 (1966).

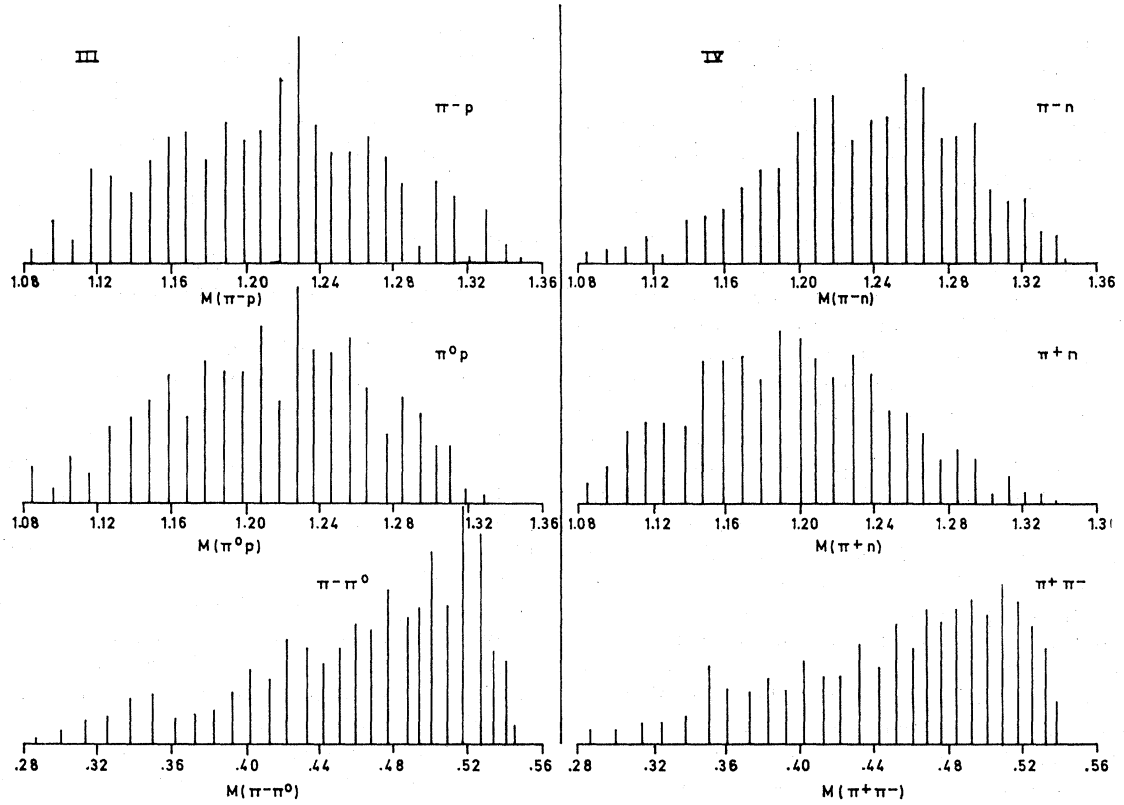

FIG. 13. Effective-mass plots for reactions III and IV at 558 MeV (from Ref. 31). [The published data are in the form of Q-value plots (essentially mass-squared plots) and these were suitably transformed.] All masses are in GeV.

ple P-wave πN^*. Centrifugal factors would then guarantee the behavior at threshold previously mentioned.

We now turn to D_{13}. As has been remarked, the OY model achieved a number of successes with the assumption of the predominant decay mode S-wave πN^*. Let us see to what extent the successes can be preserved with a value of the production cross section in line with the EPS predictions. Consider again the data at 558 MeV.[31] As we said earlier, the production angular distributions for $\pi^+\pi^- n$ were successfully explained; those for $\pi^-\pi^0 p$ not so. This was achieved with D_3 πN^* S-wave production distributed among the production channels roughly thus:

$$\sigma(\mathrm{I}) = 2.1 \text{ mb}, \ \sigma(\mathrm{II}) = 0.35 \text{ mb}, \ \sigma(\mathrm{III}) = 2.9 \text{ mb},$$
$$\sigma(\mathrm{IV}) = 4.75 \text{ mb}, \ \sigma(\mathrm{V}) = 2.65 \text{ mb}.$$

The contributions to $\pi^- p \to \pi\pi N$ are then 0.8 mb from $I = \frac{3}{2}$ and 8.5 mb from $I = \frac{1}{2}$. As stated above, we propose to retain the OY description of the D_{33} amplitude. For D_{13}, a reasonable contribution to $\sigma(\pi^- p)$ would be ~ 4.0 mb. The next question is how might this production be distributed between channels III, IV, and V. Suppose we follow OY and assume $D_{13} \to \pi N^*$ S wave. There is then the possibility of substantial interference influencing the branching ratios. If we assume no over-all

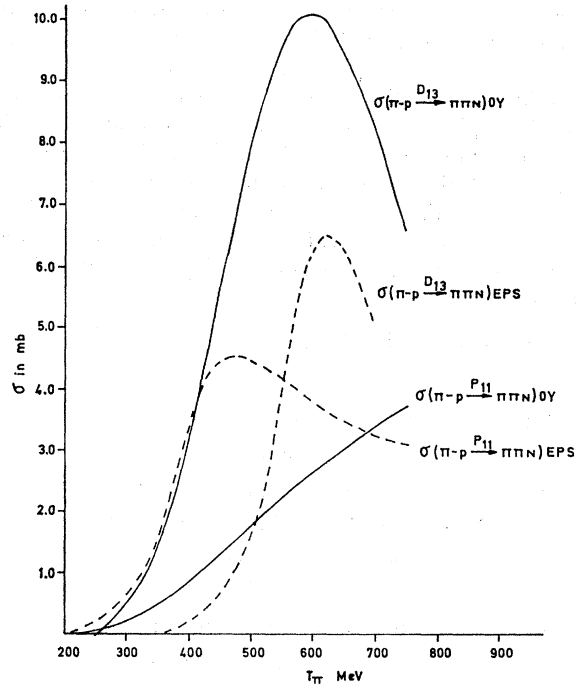

FIG. 14. Comparison of form assumed for $\sigma(\pi^- p \to \pi\pi N)$ via D_{13} and P_{11} (a) in the OY analysis (full line), (b) from the elastic phase-shift (EPS) analysis (dashed line).

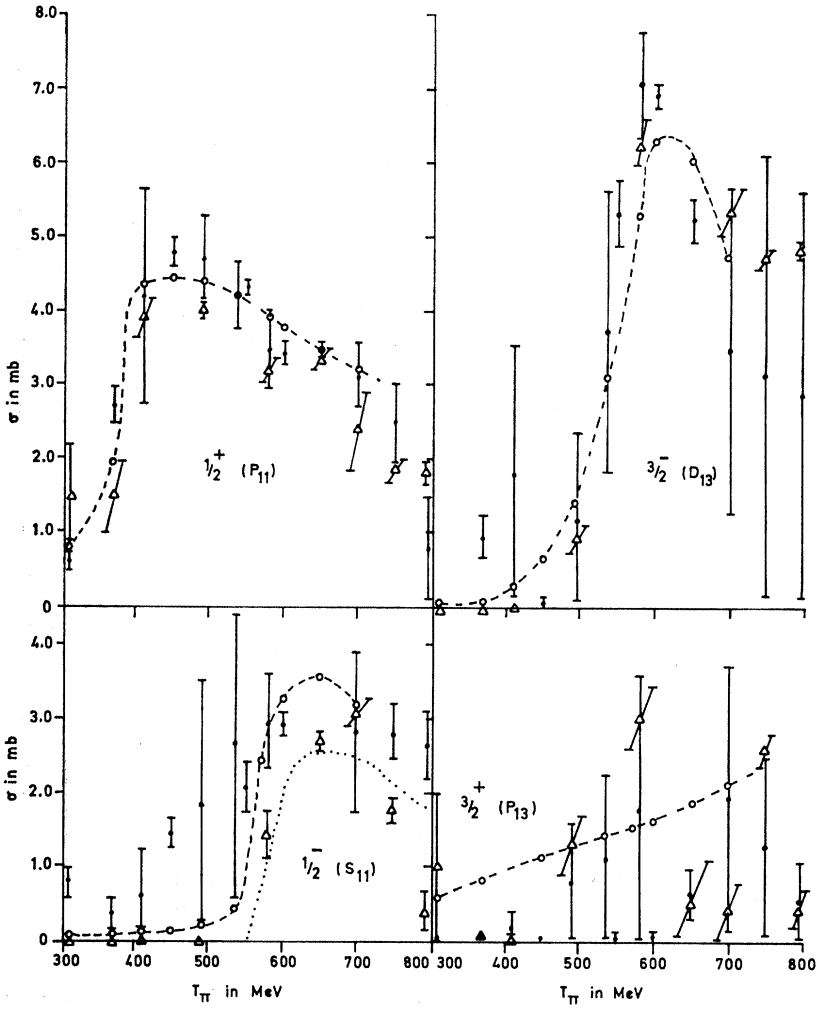

FIG. 15. $I=\frac{1}{2}$ partial-wave contributions to $\sigma(\pi^- p \rightarrow$ inelastic channels) according to three recent EPS analyses. Legend: o, Bransden *et al.*, (Ref. 28); △, Bareyre *et al.*, (Ref. 29); ●, Donnachie *et al.*, (Ref. 43). The dotted curve superimposed on the plot for $\frac{1}{2}^-$ is a fit by eye to production data on $\pi N \rightarrow \eta N(\eta \rightarrow 2\gamma)$ (see Ref. 38) assuming $(\eta \rightarrow 2\gamma)/(\eta \rightarrow$ all$) = 0.37$.

interference between $(\pi_1 N)\pi_2$ and $(\pi_2 N)\pi_1$, the formulas are

$$\sigma(\mathrm{III}) = (2/9)\sigma(1) + (17/45)\sigma(3) - (5/9)\left[\frac{2}{\sqrt{5}}\right][\sigma(1)\sigma(3)]^{1/2}\cos\Phi_1,$$

$$\sigma(\mathrm{IV}) = (5/9)\sigma(1) + (26/45)\sigma(3) + (7/9)\left[\frac{2}{\sqrt{5}}\right][\sigma(1)\sigma(3)]^{1/2}\cos\Phi_1, \tag{5.2}$$

$$\sigma(\mathrm{V}) = (2/9)\sigma(1) + (2/45)\sigma(3) - (2/9)\left[\frac{2}{\sqrt{5}}\right][\sigma(1)\sigma(3)]^{1/2}\cos\Phi_1.$$

Suppose we assume that D_{13} is a simple one-level resonance with no background and that the D_{33} production phase is zero. Then Φ_1 should equal the elastic phase and rise through 90° at about 620 MeV rather than at 500 MeV as assumed by OY. This has the effect of enhancing the branching ratio to channel IV below resonance (see Fig. 21). In particular, at 550 MeV, the D_3 contributions now lead to branching ratios.

$$\sigma(\mathrm{III}) = 0.45,\ \sigma(\mathrm{IV}) = 3.74,\ \sigma(\mathrm{V}) = 0.63.$$

When the D_3 production cross sections to channels III, IV, and V thus calculated are subtracted from the totals from all partial waves, the remainder fail at many energies to satisfy the inequalities implied by isotopic spin discussed earlier. Therefore the model cannot be correct in detail. Nonetheless we will accept the general picture of an enhanced branching ratio to channel IV below 600 MeV. This will carry the implications of a larger ratio $R = \sigma(1^{1/2})/\sigma(0^{1/2})$ for the remaining partial waves.

We have thus a plausible mechanism for understanding why $D_{3/2}$ (πN^*) goes to channel IV much as pictured by OY. But what is to take its place in channel III? Points to note are the following: (i) We need to achieve approximate isotropy—this suggests that barring cancellations there should be a fair contribution from states

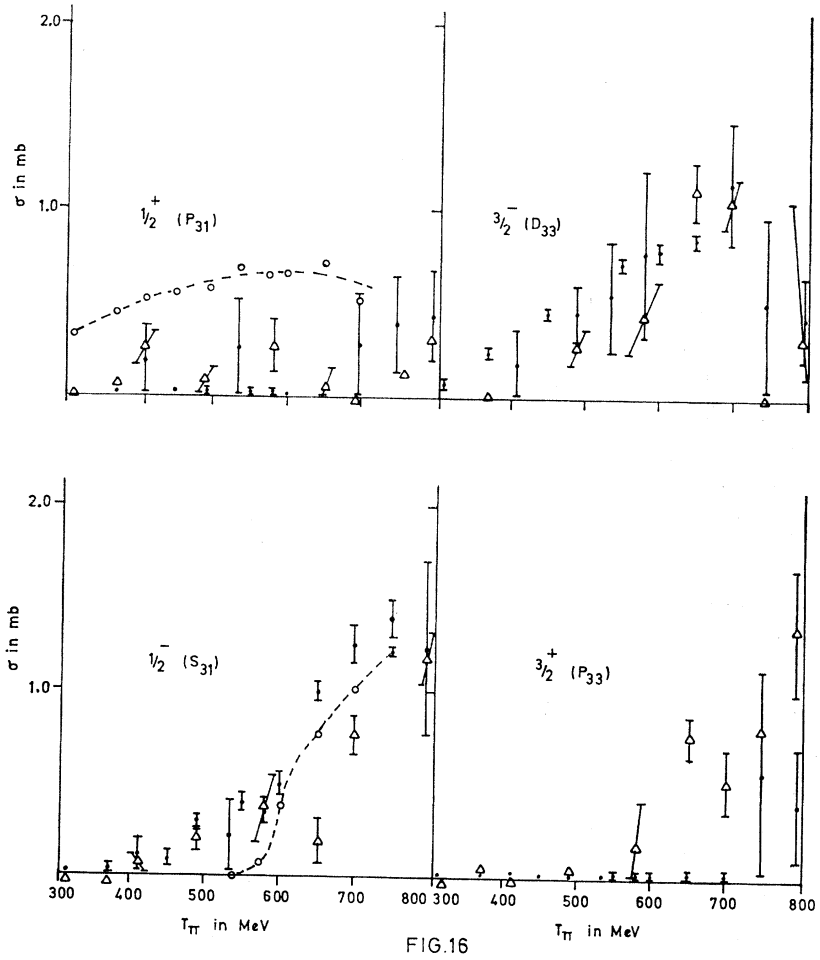

FIG. 16. $I=\frac{3}{2}$ partial-wave contributions to $\sigma(\pi^- p \to$ inelastic channels) according to three recent EPS analyses. Legend: o, Bransden *et al.*, (Ref. 28); △, Bareyre *et al.*, (Ref. 29); ●, Donnachie *et al.*, (Ref. 43).

of $J=\frac{1}{2}$ especially P_{11}; (ii) our natural explanation for the preponderance of events at the top end of the $\pi^-\pi^0$ mass spectrum has disappeared. We thus have a "Kirz anomaly" for $\pi^-\pi^0$ as well as $\pi^+\pi^-$.

We seek mechanisms which predict a large branching ratio to channel III. Natural candidates are $P_{11} \to \rho N$ (P state), $S_{11} \to \rho N$ (S state). Let us consider $P_{11} \to \rho N$ in more detail. With the parameter values listed in Sec. IV, the $\pi^-\pi^0$ mass plots are as shown in Fig. 22. (We show also the results for $S_{11} \to \rho N$). It will be noted that the calculated spectrum from $P_{11} \to \rho N$ is not as sharp as the experimental one (Fig. 14). Further sharpening can be achieved by interference with $P_{11} \to \pi N^*$ with suitably chosen production phases, or by adjusting the range parameter K_ρ.

As mentioned in Sec. IV, ρN has two P-wave couplings to $\frac{1}{2}^+$, $P_1^{(4)}=(\sigma\cdot\hat{q}_A)(\hat{q}_{12}\cdot\hat{q}_3)$ and $P_1^{(5)}=-i(\sigma\cdot\hat{q}_A)\times(\sigma\cdot\hat{q}_3\times\hat{q}_{12})$. These each give characteristic distributions with respect to $\cos\theta_3(=\hat{q}_{12}\cdot\hat{q}_3)$, i.e., across the Dalitz plot for fixed ω_{12}. The distributions are, respectively, $\cos^2\theta_3$ and $\sin^2\theta_3$. The first form gives an unwanted depletion of events in the center of the Dalitz plot so we consider only the second. The πN mass plot for this amplitude is shown in Fig. 22(a). It will be seen that it gives quite a reasonable fit to the $\pi^- p$ and

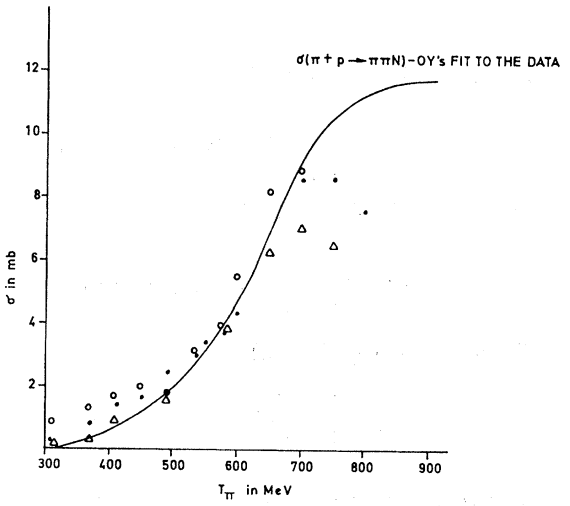

FIG. 17. $\pi^+ p$ total production cross section. Comparison of EPS predictions with the OY fit to the observed single-pion production cross sections. Legend: o, Bransden *et al.*, (Ref. 28); △, Bareyre *et al.*, (Ref. 29); ●, Donnachie *et al.*, (Ref. 43).

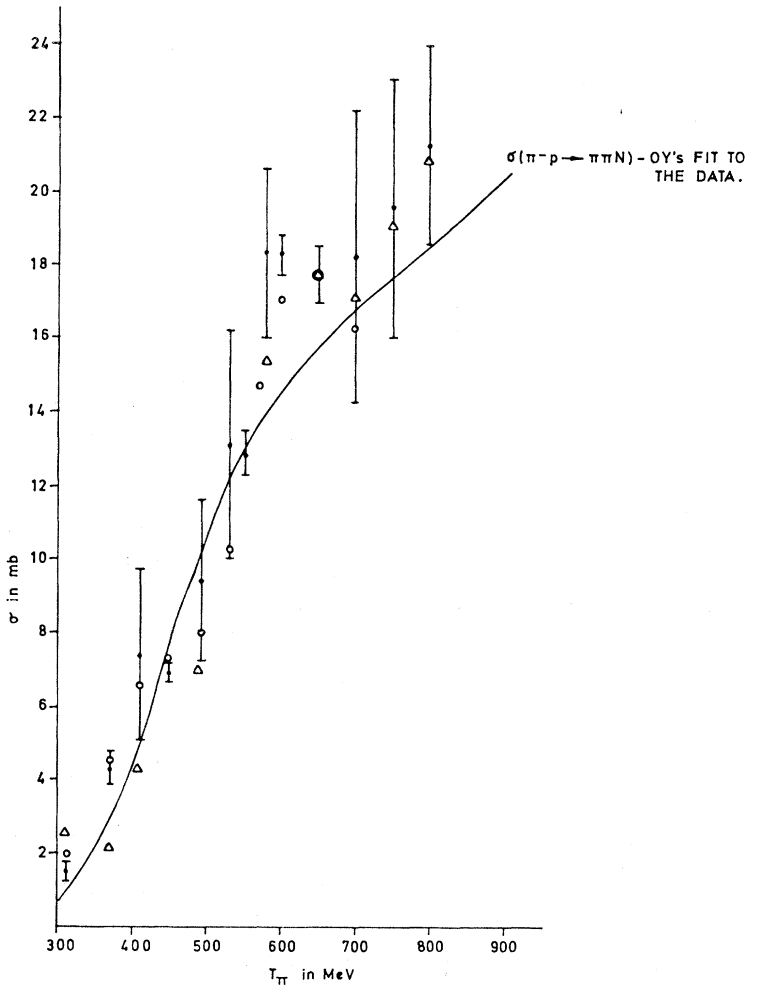

FIG. 18. $\pi^- p$ total production cross section. Comparison of EPS predictions with the OY fit to the observed single-pion production cross sections. Errors are computed from the published diagonal errors on the η's and δ's. Legend: o, Bransden *et al.*, (Ref. 28); △, Bareyre *et al.*, (Ref. 29); ●, Donnachie *et al.*, (Ref. 43).

$\pi^0 p$ experimental mass spectra. Some admixture of D_3 πN^* such as our picture already requires would slightly improve the fit. A general observation: *It is very difficult to separate πN^* from mass spectra alone.*

One can extract from the Dalitz plot for $\pi^-\pi^0 p$, the distribution in decay angle $\cos\theta_3$ of events for bands of $\pi\pi$ mass squared. We term this a $(\cos\theta_3,\omega_{12}^2)$ plot. The result, Fig. 23, is not similar to that which would be obtained for D_3 πN^* (Fig. 24); nor is it entirely compatible with $\sin^2\theta_3$. A noninterfering (out of phase) mixture of S_{11} (ρN) and P_{11} (ρN) to give $A+B\sin^2\theta_3$ would fit the data. As to the phase of S_{11}, Davies and Moorhouse[38] have made a three-channel fit with πN, ηN, σN to the data on $\pi N \to \eta N$ and the elastic phase shifts. Evaluating the parameters for their solution C, one obtains at 558 MeV arg $T(\pi N \to \pi N) \simeq 38°$, arg$T$-$(\pi N \to \sigma N) \simeq 44°$, i.e., the production phase is close to the elastic phase. Assuming that the same would hold for arg $T(\pi N \to \rho N)$, we infer that in order to get noninterference we would like arg $T(P_{11} \to \rho N) \sim 135°$.

Discussion of $\pi^+\pi^- n$ Dalitz Plot at 558 MeV

We can form the $(\cos\theta_3,\omega_{12}^2)$ plot for channel IV at 558 MeV (see Fig. 25). The result is a striking forward-backward asymmetry of the $\cos\theta_3$ distribution especially for the lower values of ω_{12}^2. (The $\cos\theta_3$ asymmetry persists at 604 and 646 MeV.) In the over-all $\cos\theta_3$ distribution, the forward-backward asymmetry is 2:1. Let us make the assumption that such a pattern obtains for the D_3 contribution, which is known to be a major although probably not predominant component. We can now make a comparison with predictions of the model for different decay patterns. If we assume D_3 goes entirely to S-wave πN^* with the $I=\frac{1}{2}$ and components deduced earlier, we obtain the distributions shown in Fig. 26. The result is an essentially symmetric distribution in $\cos\theta_3$. The origin of this is easy to understand qualitatively. The N^* bands at this energy go approximately across the middle of the Dalitz plot. To proceed further, it is convenient to make a partial-wave analysis in $\cos\theta_3$. This is equivalent to computing the recoupling coefficients $\langle(12)3|(23)1\rangle$ discussed by Wick[7] for a

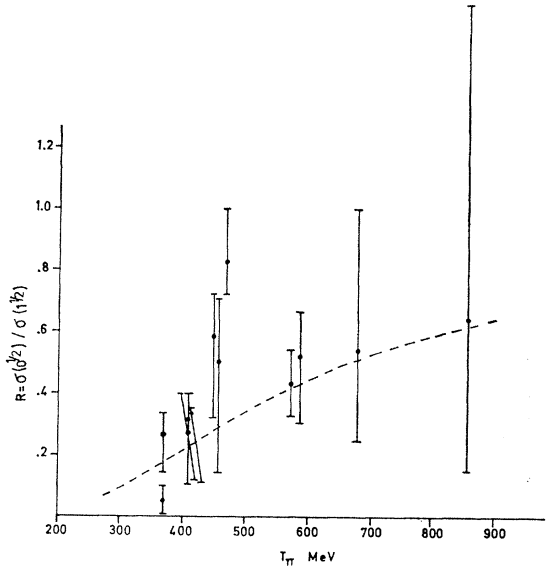

FIG. 19. Estimate of $R=\sigma(1^{1/2})/\sigma(0^{1/2})$ as a function of energy. Error bars denote limits allowed by $|X^{(\pm)}|<1$ (see text). The dots show the nearest allowed position to that corresponding to $X^{(+)}=X^{(-)}=0$.

special case. We are to take the N^* production amplitude, say, for π^+N^{*-} for fixed ω_{12}^2, varying $\cos\theta_3$ and make a Legendre analysis. The modulus of the function peaks approximately about the center of its range and the phase increases passing through 90° at the center. (Here we discuss the decay phase; the production phase is an over-all multiplicative factor.) Thus the P_0 projection is predominatnly imaginary and the P_1 projection predominantly real. We infer that suitable candidates to achieve the required interference are either a real S wave or an imaginary P wave. We select the former as being the more likely and are thus led to consider the situation where $D_{13}\to\pi N^*$ and σN. Using

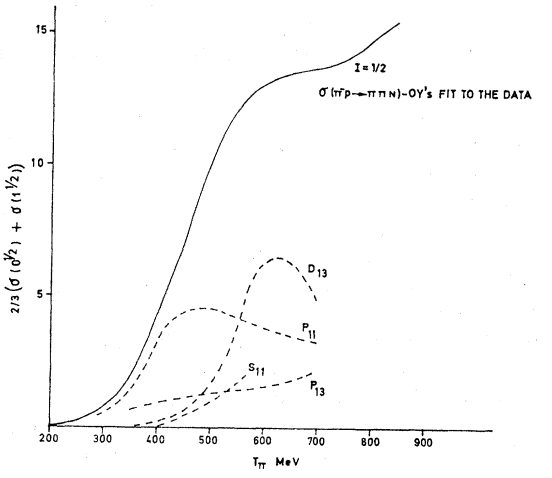

FIG. 20. Sketch of the total $I=\frac{1}{2}\pi^-p$ production cross-section and partial-wave contributions to it (rough consensus of the EPS predictions).

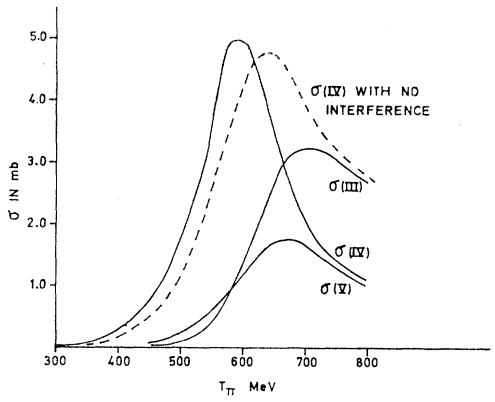

FIG. 21. D_3 branching ratios to channels III, IV, and V resulting from the hypothesis of an interfering mixture of $D_{13}\to S$-wave πN^* and $D_{33}\to\pi N^*$ (see text). The dotted curve shows the form of σ(IV) for no interference.

the σ parameters of Sec. IV, we tried various admixtures of πN^* and σN with the same and different production phases. Figure 27 shows the resulting plots for the mixture

$$D_{13}\to 0.573\pi N^*(\Phi=33.5)+0.816\sigma N(\Phi=-45°).$$

Employing equal production phases did not lead to an appreciable asymmetry, although this could presumbaly be corrected by choosing different σ parameters.

A general conslusion is that the $(\cos\theta_3,\omega_{12}^2)$ plots can be a very fruitful way of presenting the data in this energy range. One would like to know as much as possible about the dependence of this plot on the production angles.

Remarks on the P_{11}

(i) The status of the P_{11} effect as revealed in elastic scattering is unclear. It is unquestionably very inelastic up to 700 MeV and perhaps beyond. It is agreed among the EPS analysts that the phase shift arises from the zero at around 170 MeV to a value of 60–70° at 500 MeV. Thereafter ambiguity sets in—some analyses have the phase falling again, others[39] have it continuing to rise passing through 90° at about 550 MeV. The latest Berkeley tables[40] have a P_{11} resonance at 1400 MeV. ($T_{\pi\text{lab}}=430$ MeV and width 200 MeV). The resonance position is chosen from considerations of the effect of a repulsive background and the rate of description of the circle on the Argand diagram. It coincides approximately with the bump found in $p+p\to p+B^+$ missing-mass experiments.[41] If this picture is accepted, the question arises what is the substantial inelasticity above 500 MeV to be attributed to and what is the phase doing.

[39] L. D. Roper, Phys. Rev. Letters **12**, 340 (1964).
[40] A. H. Rosenfeld *et al.*, Rev. Mod. Phys. **39**, 1 (1967).
[41] G. Cocconi *et al.*, Phys. Letters **8**, 134 (1964); E. W. Anderson *et al.*, Phys. Rev. Letters **16**, 855 (1966); I. M. Blair *et al.*, *ibid* **17**, 789 (1966).

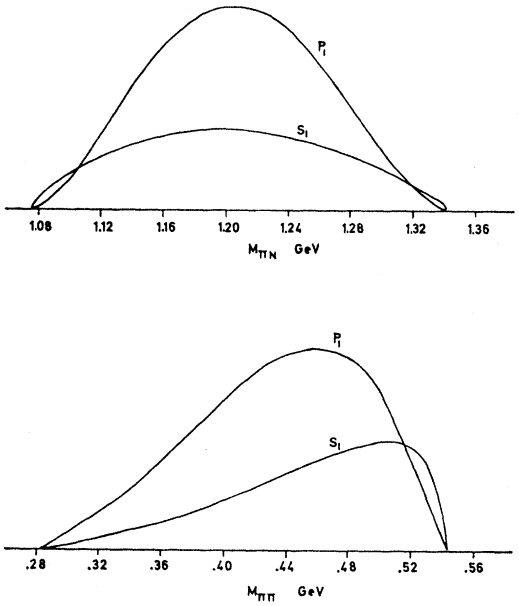

FIG. 22. Computed effective-mass plots for $P_1 \to \rho N$ and $S_1 \to \rho N$ at 558 MeV.

In an attempt to extract a little more from the phase-shift results, in particular to build in the Ball-Frazer mechanism,[42] a series of fits as a function of energy were made to DKLL Solution I[43] with the trial functions of the form

$$\frac{\ln\eta(s)}{2q^3}=\frac{Ax^2}{x+a}\prod_{i=1}^{L+1}\frac{1}{(x-y_i)^2-b_i^2}\prod_{i=1}^{L}[(x-w_i)^2+d_i^2],$$

$$\delta=\epsilon(s)+\delta_B(s)+\tfrac{1}{2}\arg\left\{\left[\prod_{i=1}^{M}\frac{(q+q_1)(q-q_i^*)^*}{(q-q_i)(q+q_i^*)}\right]\times\left[\prod_{i=1}^{N}\left(-\frac{q+ip_i}{q-ip_i}\right)\right]\right\}, \quad (5.3)$$

with

$$\epsilon(s)=\frac{q^3}{\pi}\int_{s_I}^{\infty}\frac{ds'}{s'-s}\left[\frac{-\ln\eta(s')}{2q'^3}\right],$$

$$\delta_B(s)=\arctan\left[\frac{Rq^3}{(s-s_1)(s-s_2)}\right].$$

In these formulas $\delta(s)$ and $\eta(s)$ are the phase-shift parameters which are to be fitted, $x=(t_\pi-170)$ MeV with t_π the lab energy and q the center-of-mass momentum. s_I is the inelastic threshold. The remaining quantities are adjustable parameters.

Representatives of two classes of fits to η and δ are shown in Fig. 28. Fit A has a single resonance, fit B has two resonances. The associated Argand plots are shown in Fig. 29 on which is also plotted for comparison the solution of Bareyre *et al.*[29] Taking the phase-shift determinations of the various groups together, one would

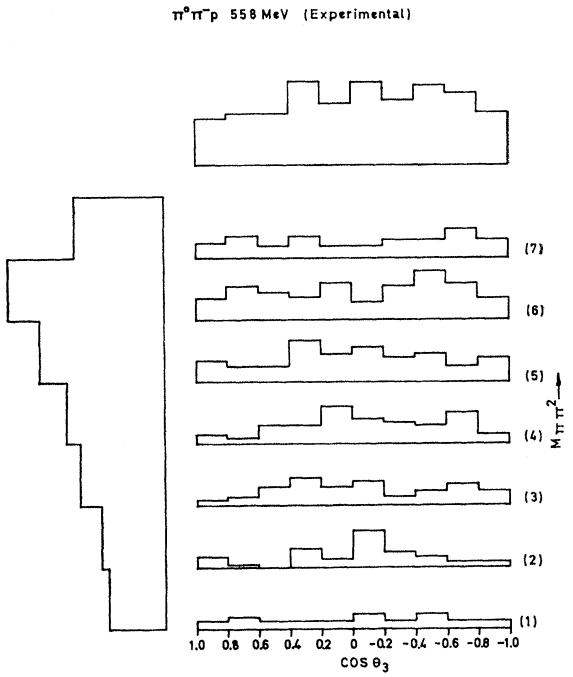

FIG. 23. Distribution of events as a function of the cosine of the decay angle, $\cos\theta_3$, for seven equal bands of $M_{\pi\pi}^2$ for reaction III at 558 MeV—experimental (Ref. 31), and total projections on the $M_{\pi\pi}^2$ and $\cos\theta_3$ axes.

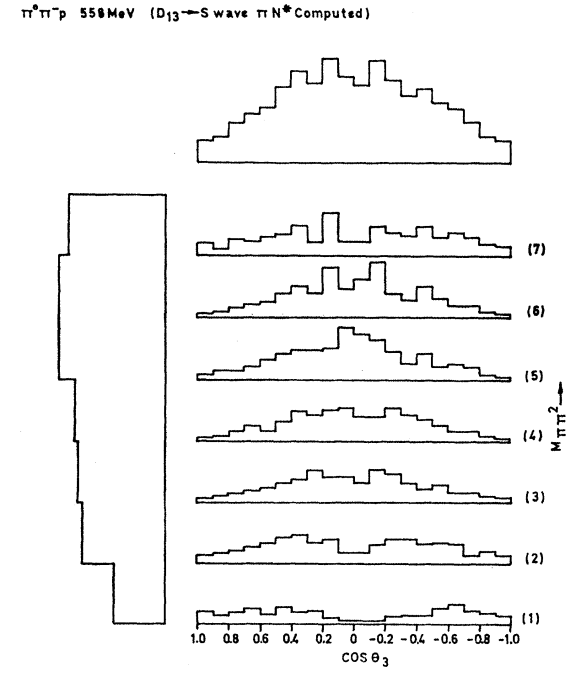

FIG. 24. $(\cos\theta_3, M_{\pi\pi}^2)$ plot as for Fig. 23. Reaction III at 558 MeV—computed for the production amplitude $D_{13} \to S$-wave πN^*.

[42] J. S. Ball and W. R. Frazer, Phys. Rev. Letters **7**, 204 (1961).
[43] A. Donnachie, *Report of Scottish Universities Summer School, 1966* (Oliver and Boyd, London, 1967), p. 330.

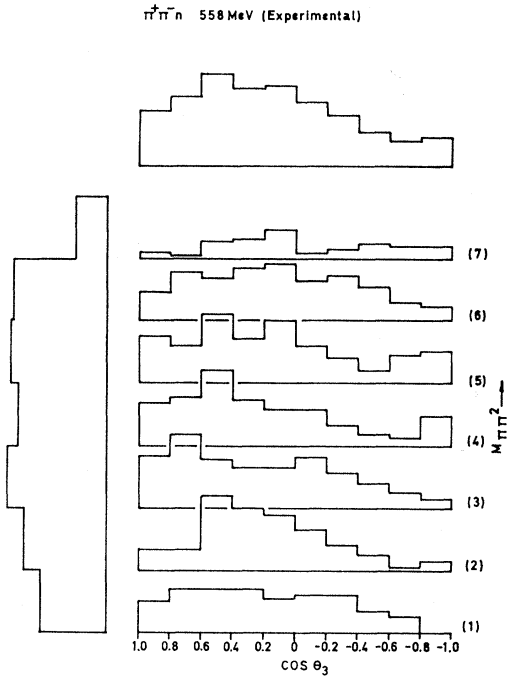

FIG. 25. $(\cos\theta_3, M_{\pi\pi}^2)$ plot as for Fig. 23. Reaction IV at 558 MeV—experimental (Ref. 31).

probably conclude that the type of solution with a single P_{11} resonance as in Fit A was the most likely but that a solution with a second resonance was not excluded. (For that matter, there are sets of phase shifts with resonance at all.[28,30])

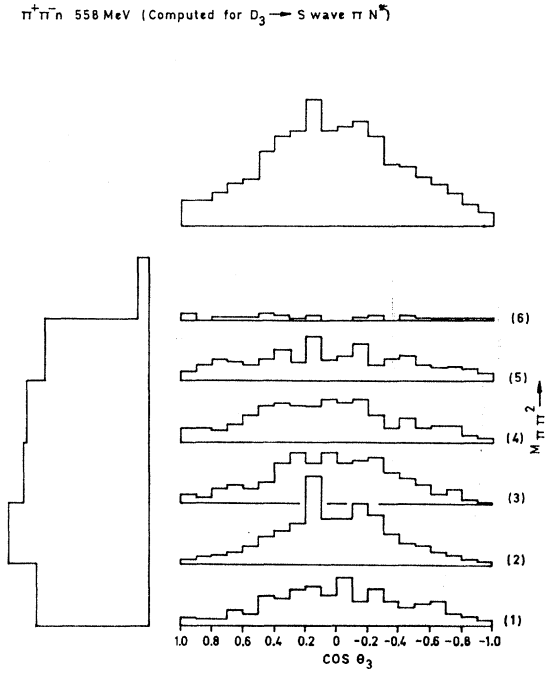

FIG. 26. $(\cos\theta_3, M_{\pi\pi}^2)$ plot as for Fig. 23 (but with six mass squared bands). Reaction IV at 558 MeV—computed for the production amplitude $D_3 \rightarrow S$-wave πN^*.

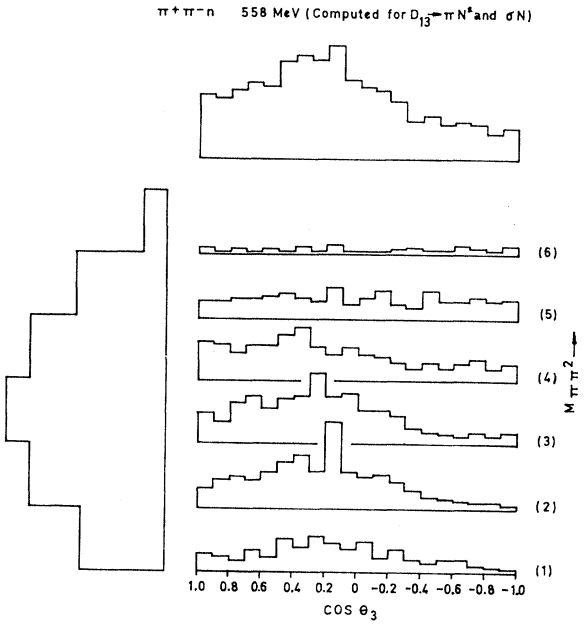

FIG. 27. $(\cos\theta_3, M_{\pi\pi}^2)$ plot as for Fig. 26. Reaction IV at 558 MeV—computed for

$$D_{13} \rightarrow 0.573|\pi N^*\rangle(\Phi=33.5°)+0.816|\sigma N\rangle(\Phi=-45°).$$

(ii) What about the inelastic data? In order to get evidence on the production phase, one needs to see an interference with other partial waves. We have already argued on tenuous grounds from the isotropy and form of the Dalitz plot in channel III for a phase of about 135° in $T(P_{11} \rightarrow \rho N)$. Another interesting set of data is provided by Kirz *et al.*[44] who plot for channel IV $(\pi^+\pi^-n)$ the forward backward asymmetry for N^{*-} production, i.e., events with $M(\pi^-n)$ between 1188 and 1288 MeV. Their results are reproduced in Fig. 30(a). One asks how is the change of sign of the forward-backward asymmetry to be interpreted. Obviously, an interference between states of opposite parity is required. The possibilities considered here are for negative-parity states S_1 and D_3 and for positive-parity P_1 and P_3. At first sight, the interpretation is clear. One is seeing the resonating D_{13} interfere with a nonresonant state of the opposite parity. However, our main positive-parity candidate is P_{11} and this is supposed itself to have a resonance. Arguing thus, one is forgetting about final-state interactions which may be different for the two states in question (also about possible quite large contributions from S_{11} and P_{13}; these could be crucial since interference effects are concerned with amplitudes rather than their modulus squared. Nonetheless, we continue to forget about these states). Let us try to form a picture of how the observed behavior of the N^{*-} asymmetry could arise through a P_1, D_3 interference. First, assume the picture of D_3 as predominantly S-wave

[44] J. Kirz, J. Schwartz, and R. Tripp, Phys. Rev. **130**, 2481 (1963).

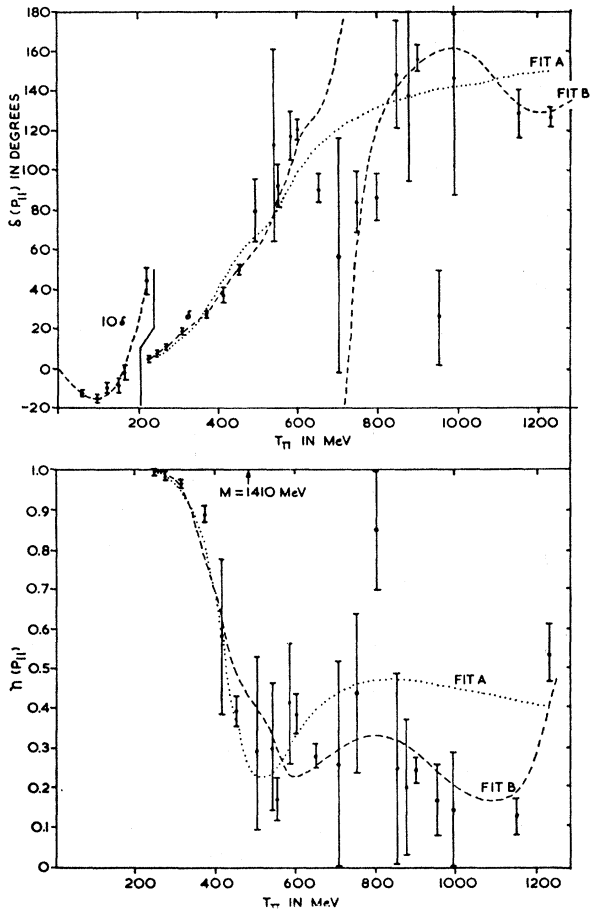

FIG. 28. Fits A and B by the trial function [Eq. (5.3)] to the phase-shift parameters $\delta(P_{11})$ and $\eta(P_{11})$ of DKLL (Ref. 43).

πN^* with constructive interference in channel IV between D_{13} and D_{33} below resonance. Calculating with the numbers already discussed, we obtain for Δ_1, the production phase in channel IV, the form shown in Figure 30(b). For purposes of illustration, we will discuss two distinct models for P_{11} production: (i) all P-wave πN^*, (ii) all S-wave σN. For case (i) the decay phases are coherent and so cancel. For case (ii), we have to allow for the decay phase in the N^* band for D_3. One can do this approximately by forming the average over the available portion of the N^* band as a function of energy $\langle\delta_{33}\rangle$ [Fig. 30(b)]. This quantity is now to be added to the production phase Δ_1, and it is the sum $\bar{\Delta}=\Delta_1+\langle\delta_{33}\rangle$ with which the phase of the P_{11} amplitude (production+decay phase) is to interfere. Making rough allowance for "efficiency factors" (i.e., the over-all production cross sections for P_{11} and D_{13} to channel IV, times relative probability of production being in the N^* band), we deduce as a suitable interference phase ϵ the form shown in Fig. 30(c) corresponding to the fit to the data shown as the dashed curve in Fig. 30(a). We are thus led to a picture of the P_{11} production phase (+ decay phase which we assume small) as being of one

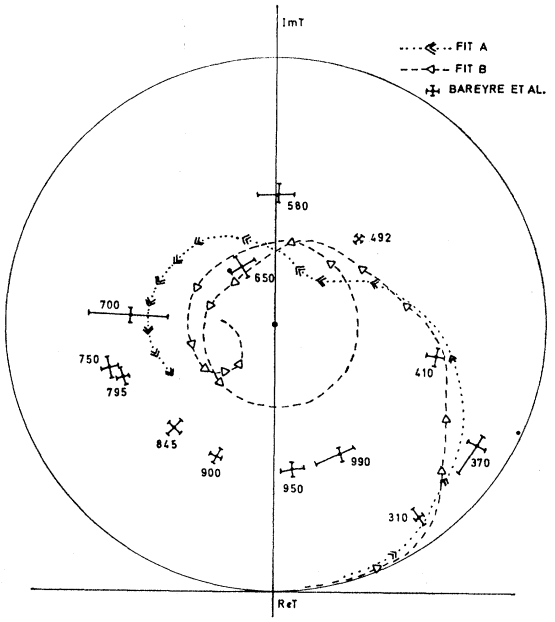

FIG. 29. Argand plot of $(\eta e^{2i\delta}-1)/2i$ for fits A and B (Fig. 28). The arrows are at 50-MeV intervals starting at 300 MeV. Points corresponding to the solution of Bareyre *et al.* (Ref. 29) are shown.

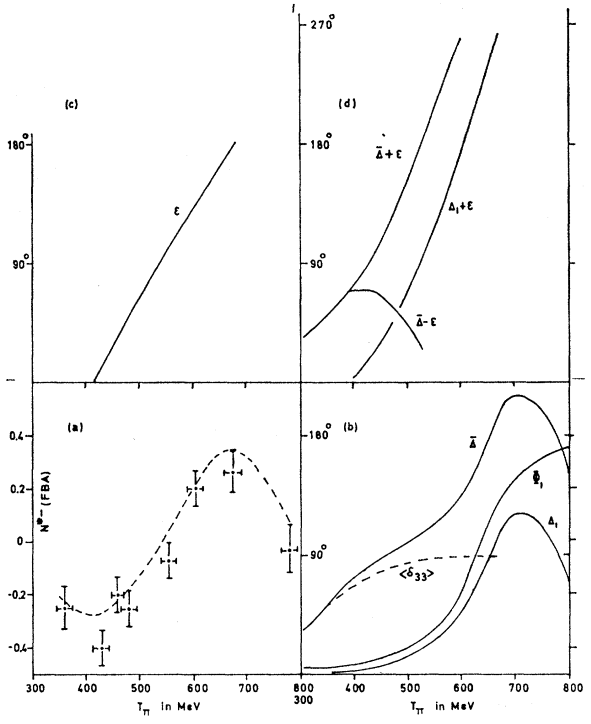

FIG. 30. (a) Forward-backward asymmtery of events in the N^{*-} band for reaction IV as a function of energy. Experimental points for Kirz *et al.* (Ref. 44) and approximate fit (dotted curve). (b) Plots of phases Φ_1, Δ_1, $\langle\delta_{33}\rangle$, and $\bar{\Delta}$ (see text) as a function of energy. (c) assumed form of the interference phase ϵ as a function of energy. (d) Alternative solutions for P_{11} production phase as a function of energy.

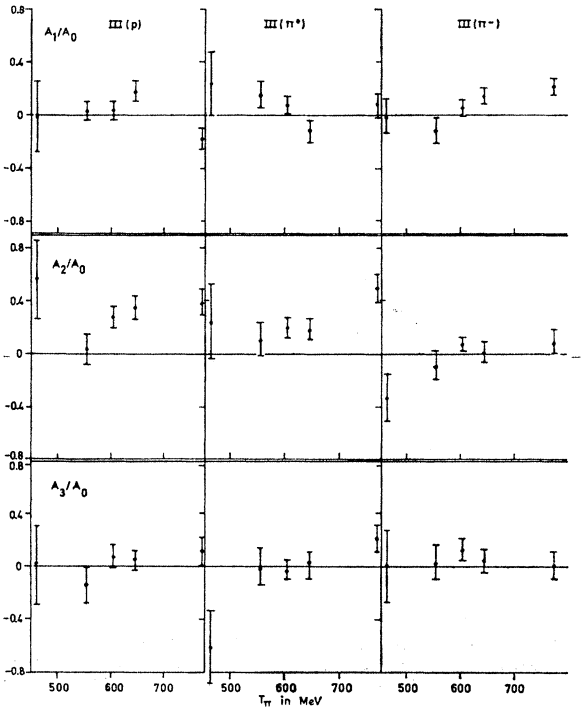

FIG. 31. Relative Legendre coefficients as a function of energy for production angular distrubutions for reaction III.

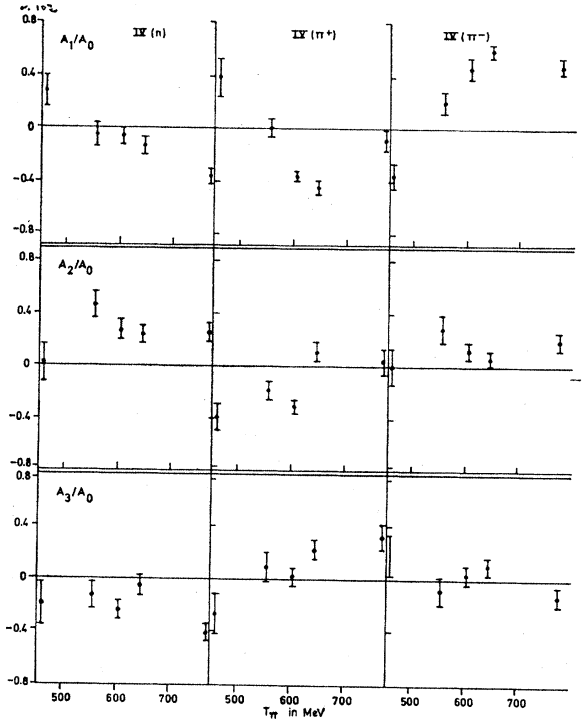

FIG. 32. Relative Legendre coefficients as a function of energy for production angular distributions for reaction IV.

of the three forms shown in Fig. 30(d). Evidently, there is scope for a lot of phase variation of P_{11} including a second resonance, although this is obviously very far from being a unique explanation. For example, one could have the solution $\bar{\Delta}-\epsilon$ [Fig. 30(d)] in which the phase rises to a high value below 90° and then falls. This resembles some of the elastic phase-shift determinations.[28,30]

In discussion of both the elastic and inelastic data we have been led to note the possibility of a second P_{11} resonance occurring somewhere in the range 600–800 MeV. It should be strongly coupled to what we have termed the ρN channel. Being a distinct structure from the lower resonance at 1410 MeV, it could very well have different production properties at high energies.

The question of the existence of a P_{11} resonance (and *a fortiori* of two resonances) is of interest in the quark model since there would be difficulties in finding a quark configuration to which it would naturally belong.[45] It may be that in situations where long-range forces (one-pion exchange) dominate, there exist bound states and resonances which do not have supermultiplet companions. It seems that the deuteron may be one such.[46]

[45] R. H. Dalitz, in *Proceedings of the Thirteenth Annual International Conference on High-Energy Physics, Berkeley, 1966* (University of California Press, Berkeley, 1967), p. 233.

[46] The question of a possible dibaryon supermultiplet to contain the deuteron has been discussed by R. J. Oakes, Phys. Rev. **131**, 2239 (1963).

Partial-Wave Contributions to the Charge Channels and Production Angular Distributions

Thus far we have obtained a general picture of what happens to the P_{11} and D_{13} contributions. We now summarize these conclusions and briefly review the other partial-wave contributions. We also examine more systematically the data on production angular distributions.

In order to fix ideas, we extract from the partial-wave analyses a rough average of the partial-wave production cross sections for $T_\pi=558$, 604, and 646 MeV. These are set forth in Table V, the numbers being contributions to $\sigma(\pi^- p \to \pi\pi N)$ in mb. We have already discussed a model for the charge branching ratios for D_3. What can we say for P_1? We have argued for a fair-sized branching ratio to the channel III. As a guess, let us fix on 50%. If we then assume that P_{11} decays entirely to ρN, πN^*, and σN in the proportions $r_1:r_2:r_3$, we derive (assuming as before no over-all interference between the two N^* bands)

$$\sigma(\mathrm{III}):\sigma(\mathrm{IV}):\sigma(\mathrm{V})=[\tfrac{2}{3}r_1+(2/9)r_2] :[\tfrac{1}{3}r_1+(5/9)r_2+\tfrac{2}{3}r_3]:[(2/9)r_2+\tfrac{1}{3}r_3]. \quad (5.4)$$

It follows that no matter what the ratio of $r_2:r_3$, we obtain

$$\sigma(\mathrm{III}):\sigma(\mathrm{IV}):\sigma(\mathrm{V})=\tfrac{1}{2}:5/12:\tfrac{1}{12} \quad (5.5)$$

We are left with P_3 and S_1 to apportion. Let us arbitrarily assume that they split as for the πN^* decay

TABLE V. Partial-wave contributions to $\pi^- p \to \pi\pi N$ in mb (rough average of the EPS predictions).

T_π (MeV)	$\frac{1}{2}^-$ $I=\frac{1}{2}$	$\frac{1}{2}^-$ $I=\frac{3}{2}$	$\frac{1}{2}^+$ $I=\frac{1}{2}$	$\frac{1}{2}^+$ $I=\frac{3}{2}$	$\frac{3}{2}^+$ $I=\frac{1}{2}$	$\frac{3}{2}^+$ $I=\frac{3}{2}$	$\frac{3}{2}^-$ $I=\frac{1}{2}$	$\frac{3}{2}^-$ $I=\frac{3}{2}$	Total estimated from production experiments	Total from phase shifts
558	2.0	0.1	4.2	0.5	1.5	0.1	4.3	0.7	13	13.4
604	1.0–2.0	0.4	3.8	0.6	1.7	0.2	6.5	0.8	14.5	15–16
646	1.0–2.0	0.8	3.4	0.6	1.9	0.4	6.0	1.0	15.5	15–16

modes, i.e., in the ratio (2/9):(5/9):(2/9). We then obtain the pattern set forth in Table VI.

We now have a hypothesis for the distribution of the partial waves among the charge states. It essentially fits the total cross sections to the charge channels. It is to be noted that the S_1 and P_3 contributions are far from negligible and are necessary to get agreement with the observed totals. One would like to have evidence that it is these particular partial waves that are present. For this we have to await more extensive data.

We now turn to the information on production angles. The experimental data is presented in the form of distributions $d\sigma/d(\cos\Theta_i)$ and we have extracted the coefficients A_l in a Legendre expression $\sum A_l P_l(\cos\Theta_i)$. We state the formula for the A_l in terms of partial-wave production amplitudes which are derived in Appendix B:

$$\begin{aligned} A_0 &= |s_1|^2+|p_1|^2+|d_3^{(1)}|^2+|d_3^{(2)}|^2 \\ &\quad +|p_3^{(1)}|^2+|p_3^{(2)}|^2, \\ A_1 &= 2\,\mathrm{Re}[p_1^*\cdot s_1-\sqrt{2}(p_1^*\cdot d_3^{(2)}-s_1^*\cdot p_3^{(2)}) \\ &\quad +\tfrac{3}{5}(p_3^{(1)*}\cdot d_3^{(1)}-\tfrac{1}{3}p_3^{(2)*}\cdot d_3^{(2)})], \quad (5.6) \\ A_2 &= \mathrm{Re}[|d_3^{(2)}|^2-|d_3^{(1)}|^2+|p_3^{(2)}|^2-|p_3^{(1)}|^2 \\ &\quad +2\sqrt{2}(p_1^*\cdot p_3^{(2)}-s_1^*\cdot d_3^{(2)})], \\ A_3 &= -3\,\mathrm{Re}[\tfrac{2}{5}p_3^{(1)*}\cdot d_3^{(1)}+(6/5)p_3^{(2)*}\cdot d_3^{(2)}]. \end{aligned}$$

The quantities s_1, p_1, $d_3^{(1,2)}$, $p_3^{(1,2)}$ are functions over the Dalitz plot and depend on the nucleon spin orientation so that products such as $p_3^{(1)*}\cdot d_3^{(1)}$ and $|p_1|^2$ are to be interpreted as vector products in a Hilbert space, i.e., spin sums and averages over the Dalitz plot. The quantities averaged are different according to which final particle is singled out as reference direction. It will be seen from the formulas for A_0 and A_2 that D_3 and P_3 have each one set of spin components which contribute positive curvature and one which contributes negative curvature.

We now review the data. This is set forth in Figs. 31 and 32 and Table VII in which the quantities plotted are A_1/A_0, A_2/A_0, and A_3/A_0 for reactions III and IV with appropriate statistical errors. We use the notation for example IV(n) to denote the distribution in $\cos\Theta_n$ for channel IV. In order to show trends as a function of energy, we have included as well as the data for 558, 604, and 646 MeV[31–33] also that for 775 MeV[47] and for 460 MeV.[48] We note the following points:

(i) For channel IV, A_2/A_0 is comparatively large and positive at 558 MeV and thereafter decreases as the energy rises for the distributions IV(n) and IV(π^-). For IV(π^+) the data points have a more complicated pattern and are possibly compatible with a value remaining fairly close to zero.

(ii) For channel III, A_2/A_0 is close to zero at 550 MeV for III(π^0), III(π^-), and III(p). The latter shows a systematic increase for higher energies.

(iii) For channel IV, the ratio A_1/A_0 shows a pronounced variation with energy for IV(π^+) and IV(π^-), whereas IV(n) stays close to zero over the range 550 to 650 MeV.

(iv) For channel III, the corresponding coefficients show much less change.

(v) Only at 775 MeV for channel IV is the ratio A_3/A_0 significantly different from zero.

We have computed some values of A_2/A_0 for different isobar configurations for the case $T_\pi=558$ MeV. (We do not expect a lot of variation with energy say between 550 and 650 MeV.) The results are shown in Table VIII.

TABLE VI. Possible branching ratios of the partial waves to $\pi^0\pi^- p$(III), $\pi^+\pi^- n$(IV), and $\pi^0\pi^0 n$(V), all in mb.

	558 MeV III	558 MeV IV	558 MeV V	604 MeV III	604 MeV IV	604 MeV V	646 MeV III	646 MeV IV	646 MeV V
D_3[a]	0.45	3.74	0.63	1.35	4.95	1.15	2.7	3.4	1.7
P_1	2.35	1.9	0.45	2.2	1.8	0.4	2.0	1.67	0.33
P_3	0.35	0.9	0.35	0.4	1.1	0.4	0.5	1.3	0.5
S_1[b]	0.45	1.1	0.45	0.4±0.1	1.1±0.3	0.4±0.1	0.5	1.3	0.5
Total	3.6	7.6	1.9	4.4	9.0	2.4	5.7	7.7	3.0
Expt.	4.0±0.5	7.5±0.8		4.98±0.54	7.87±0.91		4.65±0.27	7.4±0.23	

[a] The D_3 branching ratios cited are for the S-wave πN^* D_{13} and D_{33} model discussed earlier. The pattern $D_{13} \to 0.57\pi N^* + 0.82\sigma N$ with phase difference developed to explain the channel IV Dalitz plot alters the ratios at 558 MeV to 0.16:3.56:1.10.
[b] It is hard to estimate the amount of S_1 because of uncertainties as to the normalization of η production. We take a rough average.

[47] L. Bertanza, A. Bigi, R. Carrata, and R. Casali, Nuovo Cimento 44A, 712 (1966).
[48] C. P. Poirier *et al.*, Phys. Rev. 148, 1311 (1966).

TABLE VII. Relative Legendre coefficients in the expansion of $d\sigma/d\cos\Theta_i$ for reactions III and IV.

T_π (MeV)	Reaction	No. of Events	1 A_1/A_0	1 A_2/A_0	1 A_3/A_0	2 A_1/A_0	2 A_2/A_0	2 A_3/A_0	3 A_1/A_0	3 A_2/A_0	3 A_3/A_0
460	III	100	0.24±0.24	0.23±0.29	−0.62±0.29	−0.01±0.14	−0.35±0.19	0.0 ±0.27	−0.01±0.27	0.57±0.31	0.13±0.30
556	III	441	0.16±0.10	0.12±0.12	0.01±0.14	−0.11±0.09	−0.09±0.11	0.03±0.13	0.03±0.10	0.04±0.12	−0.14±0.14
604	III	1316	0.08±0.06	0.20±0.08	−0.03±0.08	0.05±0.06	0.07±0.07	0.13±0.04	0.03±0.07	0.28±0.08	0.08±0.08
646	III	1049	−0.12±0.07	0.19±0.08	0.02±0.09	0.14±0.06	0.00±0.08	0.04±0.09	0.19±0.08	0.36±0.09	0.04±0.09
775	III	833	0.08±0.09	0.49±0.11	0.21±0.10	0.22±0.07	0.09±0.09	0.00±0.10	−0.18±0.10	0.39±0.10	0.11±0.10
460	IV	325	0.39±0.14	−0.38±0.10	−0.27±0.15	−0.35±0.11	0.00±0.14	0.18±0.16	0.28±0.11	0.02±0.14	−0.20±0.16
556	IV	848	0.0 ±0.07	−0.18±0.07	0.09±0.10	0.20±0.08	0.29±0.10	−0.09±0.10	−0.05±0.09	0.46±0.10	−0.13±0.10
604	IV	1841	−0.35±0.03	−0.30±0.05	0.01±0.06	0.47±0.05	0.13±0.06	0.03±0.07	−0.06±0.06	0.28±0.07	−0.24±0.07
646	IV	1609	−0.44±0.05	0.11±0.07	0.22±0.07	0.59±0.05	0.06±0.06	0.10±0.07	−0.13±0.06	0.24±0.07	−0.05±0.07
775	IV	1598	−0.08±0.08	0.04±0.10	0.32±0.10	0.48±0.05	0.20±0.06	−0.13±0.07	−0.36±0.06	0.26±0.07	−0.41±0.07

It will be noted that the simple hypotheses for D_3 give positive curvatures whereas those for P_3 give predominantly negative curvatures. This follows from the construction of the quantities $d_3^{(1,2)}$ and $p_3^{(1,2)}$. One can check for example that the D_3 state built from σN has exactly the value 1.0 for A_2/A_0 for the case when one refers the azimuth to the nucleon direction. Other distributions are blurred through the rotation of axes but the trend to positive curvatures remains. In order to achieve negative curvature with D_3, one needs to go to more complicated configurations such as D-wave πN^*.

The A_2/A_0 values for channel IV thus support the notion of a large D_3 component. The large values for IV(n) and IV(π^-) favor the hypothesis of $D_{13} \to S$-wave πN^*. The isotopic Clebsch-Gordan coefficients are such that this is predominantly $\pi^+ N^{*-}$ resulting in approximate isotropy for π^+. A modest admixture of P-wave σN with S-wave πN^* is also compatible with the data. The decrease with energy of A_2/A_0 for IV(n) and IV(π^-) suggests a decreasing portion of D_3 in channel IV. Our model predicts a diminishing branching ratio to channel IV but this is compensated by the rising D_3 cross section. It appears that one needs some additional effect perhaps from the $s_1^* \cdot d_3^{(2)}$ interference to achieve full agreement. If we accept the broad picture set forth in Table VI with D_3 comprising only 50% of the total in channel IV, the A_2/A_0 values at 558 MeV are seen to be very large. If there is as much as 0.9 mb of P_3 contributing negative curvature, this remark holds *a fortiori*.

The increase in curvature in channel III is also in accord with our picture. That it occurs predominantly in III(p) is rather puzzling.

The trend in A_1/A_0 for channel IV reveals an energy-dependent interference effect. The behavior of this quantity for the π^+ distribution is of course closely related to the forward-backward asymmetry of N^{*-} already discussed. Once again we try to understand the effect as an interference between D_{13} and a positive-parity contribution. If this is P_{11} and is to show no asymmetry in IV(n), then we deduce from calculations that the decay channels have to take a rather special form. Thus for $D_{13} \to 0.816|\pi N^*\rangle + 0.573|\sigma N\rangle$ (in phase) we required $P_{11} \to |\pi N^*\rangle + 0.56|\sigma N\rangle - 3.18|\rho N\rangle$. P_{13} could also be playing a part.

That A_3/A_0, which can be as large as 9/5, remains small confirms the picture of D_3 being predominantly coupled to $d_3^{(2)}$ and P_3 to $p_3^{(1)}$. The rather small values of A_1/A_0 for channel III deserve mention since we seem definitely to require an admixture of opposite parity contributions for this amplitude. We have already discussed the question of S_1, P_1 interference at 558 MeV and suggested that a very large production phase for P_1 could cause this interference to be small.

VI. CONCLUDING REMARKS

We have evolved the following picture of the production phases and decay channels for the $I=\frac{1}{2}$ partial waves. (1) $D_{13} \to S$-wave πN^* with production phase as for elastic scattering. There is also evidence for the

TABLE VIII. Computed values of $A_2/A_0(\Theta_i)$ for assorted production and decay channels. Except where stated, all cases are computed for $T_\pi = 558$ MeV.

Partial wave	Decay mode	Channel IV(III)	$A_2/A_0(\Theta_1)$ $\pi^+(\pi^0)$	$A_2/A_0(\Theta_2)$ π^-	$A_2/A_0(\Theta_3)$ $n(p)$
D_{13}	S-wave πN^*	III	0.54	0.54	0.32
D_{13}	S-wave πN^*	IV	0.06	0.69	0.55
D_{13} + D_{33}	S-wave $\pi N^*(\Phi=33.5°)$; S-wave $\pi N(\Phi=0°)$	IV	−0.01	0.91	0.53
D_{13}	P-wave σN	IV	0.19	0.19	1.0
D_{13}	S-wave ρN	IV	0.66	0.66	0.0
P_{13}	P-wave πN^*	IV	−0.72	0.24	−0.29
P_{13}	P-wave πN^*	III	−0.40	−0.40	−0.40
P_{13}	P-wave ρN $(1+1=1)+\frac{1}{2}=\frac{3}{2}$ coupling				−0.50
D_{33} + D_{33} as above	πN^* and σN; πN^* S-wave (at 646 MeV)	III	0.41	0.63	0.24
		IV	0.03	0.88	0.41

following: $D_{13}\to P$-wave σN (with the σ parameters which have been employed one requires different production phases for πN^* and σN). (2) $P_{11}\to S$-wave σN below 400 MeV. Thereafter we have in addition either or both of

$$P_{11}\to P\text{-wave } \pi N^*,$$
$$P_{11}\to P\text{-wave } \rho N.$$

At 550 MeV and above, a substantial amount of the ρN decay channel seems to fit the data. It appears that a very large production phase compatible with a second P_{11} resonance would be helpful in fitting the data on forward-backward asymmetries. (3) S_{11} and P_{13} have to be present to bulk up the cross sections. We have no comment on their decay channels except the remark that a component $S_{11}\to\rho N$ could help to explain the $\pi^0\pi^-p$ Dalitz plot.

A novel conclusion of this analysis has been the emergence of $P_{11}\to\rho N$ as a significant decay mechanism. One would like to interpret the facts in as model-independent way as possible. Thus: (i) $I=\frac{1}{2}$ $\pi N\to\pi^0\pi^-p$ necessarily has $I_\pi=1$. (ii) $I_\pi=1\Rightarrow l_\pi=1, 3\cdots$ (Bose statistics). (iii) Therefore any model with $P_{11}\to\pi^0\pi^-p$ (say πN^*) has a large component of $(\pi\pi)N$ with $I_\pi=1$, $l_\pi=1$. (iv) However, it is hard to see why πN final-state interactions do not cause the cross section to leak into channel IV. We conclude that a large branching ratio of P_{11} to channel III, if confirmed, sets a challenge to theory. On the other hand, $S_{11}\to\rho N$ would be very stable against "leakage."

The whole discussion hinges critically on the elastic phase-shift analyses being broadly correct especially as to the relative inelasticities in S_1 and P_1. One awaits revised phase-shift analyses incorporating the latest polarization experiments which fortunately span the region discussed here.[49]

The idea of strong ρN coupling to P_{11} ties in with the recent pion photoproduction analysis of Chau *et al.*[50] These authors find a strong photoproduction of P_{11} persisting up to photon energies equivalent to $T_\pi\sim 700$ MeV. One can now consistently picture the photoproceeding via γ-ρ coupling.

All conclusions are more or less tentative, being flawed by the unsystematic procedures to which one is driven by the form and extent of existing data. One therefore asks how future experiments might improve matters.

Firstly, it is obviously desirable to gather data at more energies with better statistics and especially to perform experiments on as many charge channels as possible at the same energy. There is also the question of how the data should be presented (think of an experiment with 6000 events at a given energy). Up to the present, data on single-pion production has been published in the form of averages: (a) over-all Dalitz-plot distributions; (b) production angular distributions. In theoretical analysis of the experiments, one has attempted to distinguish between hypotheses by confronting their predictions with such averages. The results have been not altogether consistent and certainly not conclusive. It has been necessary to feed in extra *ad hoc* assumptions at various points. Since in a bubble-chamber experiment all kinematic variables are determined for each event, it is evident that much information is lost in the conventional presentation.

What is required is a compact way of recording correlations between the production angles and position on the Dalitz plot. This is afforded by the analysis of Arnold and Uretsky[10] which is set forth in Appendix B. According to Eq. (B4), the production intensity W has the following expansion in spherical harmonics:

$$W(\Theta,\Phi,\omega_1,\omega_2)=\sum_{jm}\left(\frac{2j+1}{4\pi}\right)^{1/2}\times Y_j^{m*}(\Theta,\Phi)W_m{}^j(s,\omega_1,\omega_2), \quad (6.1)$$

in which $W_{-m}{}^j=(-)^m W_m{}^{j*}$ and terms with odd $j+m$ vanish.

Written out for the case $J\leqslant\frac{3}{2}$, this becomes

$$W(\Theta,\Phi,\omega_1,\omega_2)=\frac{1}{4\pi}\Big\{W_0{}^0-\left(\frac{3}{\sqrt{2}}\right)P_1{}^1(\cos\Theta)[\cos\Phi\ \mathrm{Re}W_1{}^1-\sin\Phi\ \mathrm{Im}W_1{}^1]+\left(\frac{5}{\sqrt{6}}\right)P_2{}^2(\cos\Theta)$$
$$\times[\cos2\Phi\ \mathrm{Re}W_2{}^2-\sin2\Phi\ \mathrm{Im}W_2{}^2]+5P_2{}^0(\cos\Theta)W_0{}^2-\left(\frac{7}{\sqrt{180}}\right)P_3{}^3(\cos\Theta)[\cos3\Phi\ \mathrm{Re}W_3{}^3-\sin3\Phi\ \mathrm{Im}W_3{}^3]$$
$$-\left(\frac{7}{\sqrt{3}}\right)P_3{}^1(\cos\Theta)[\cos\Phi\ \mathrm{Re}W_1{}^3-\sin\Phi\ \mathrm{Im}W_1{}^3]\Big\}, \quad (6.2)$$

where the ten real functions $W_0{}^0$, $\mathrm{Re}W_1{}^1$, etc. depend on the coordinates of the Dalitz plot. They are the generalization of the Legendre coefficients employed in the description of elastic scattering experiments. They contain in principle all the information that a production experiment can give.

We therefore propose the following procedure. (a) Divide the Dalitz plot into cells. For example, we have

[49] P. J. Duke *et al.*, preliminary data presented at I.P.P.S. Conference at University College London, 1967.

[50] Y. C. Chau, N. Dombey, and R. G. Moorhouse, Phys. Rev. **163**, 1632 (1967).

found $(\cos\theta_3,\omega_{12}^2)$ to be very convenient for this purpose. (b) For each cell, determine the coefficients $W_m{}^j$ by summing events with the appropriate weighting factor:

$$W_m{}^j=\frac{4\pi}{(2j+1)^{1/2}}\int_{-1}^{1}d(\cos\theta)\int_0^{2\pi}d\Phi \times Y_j{}^m(\Theta,\Phi)W(\Theta,\Phi,\cos\theta_3,\omega_{12}^2). \quad (6.3)$$

One would extract the $W_m{}^j$'s up to whatever j value gave significant results, probably adopting a coarser mesh for the higher values. The analysis has been presented in terms of the normal coordinates Θ, Φ which seems rational and convenient. Since one is not now averaging over the Dalitz plot, the $\overline{W}_m{}^j$'s for any other system can be computed by an explicit transformation. The choice of the axis for Φ is arbitrary and could be chosen, say, as the nucleon direction. Again there exists an explicit transformation to pass from one choice to another.

Once given the detailed form of the $W_m{}^j$'s over the Dalitz plot, one would be able to make a much more careful analysis. One would still not be in such a good case as for elastic scattering, lacking polarization experiments and the extra phase information that comes from the coherence of the scattered with the incoming wave. This entails an over-all phase uncertainty $\Delta(\omega_1,\omega_2)$ in any determination of the production amplitude. Aside from this, the way would be clear for fitting the data meaningfully to a sum of partial-wave production amplitudes. Production studies could begin to approach the precision of elastic scattering analysis and fully complement them in the unraveling of resonance decay patterns

ACKNOWLEDGMENTS

The author thanks I. J. R. Aitchison, D. V. Bugg, C. Michael, and N. Dombey for illuminating conversations.

APPENDIX A: FURTHER NOTES ON THE THREE-BODY ANGULAR FORMALISM

Angles Θ, Φ, Θ_i, Φ_i, Ψ, θ_i, χ_i are defined in terms of the unit vectors $\hat{q}_A$, $\hat{q}_i$, $\mathbf{n}$, and $\hat{q}_{ij}$ introduced in Sec. II.

$$\hat{q}_A\cdot\mathbf{n}=\cos\Theta, \quad (A1)$$

$$\hat{q}_A\cdot\hat{q}_i=\cos\Theta_i, \quad (A2)$$

$$[\hat{q}_A-\cdot(\hat{q}_A\cdot\mathbf{n})\mathbf{n}]\cdot\hat{q}_i=\sin\Theta\cos(\Phi+\rho_i), \quad (A3)$$

where $\rho_i(i=1,2,3)=(0,-\chi_3,\chi_2)$ or $(\chi_3,0,-\chi_1)$ or $(-\chi_2,\chi_1,0)$ according to which $\hat{q}_i$ is taken as the reference direction.

$$\hat{q}_{ij}\cdot\hat{q}_k=\cos\theta_k, \quad (A4)$$

$$[\hat{q}_A-(\hat{q}_A\cdot\hat{q}_k)\hat{q}_k]\cdot[\hat{q}_{ij}-(\hat{q}_{ij}\cdot\hat{q}_k)\hat{q}_k] =\sin\theta_k\sin\Theta_k\cos\Phi_k, \quad (A5)$$

$$\hat{q}_i\cdot\hat{q}_j=\cos\chi_k, \quad (A6)$$

$$\mathbf{s}_x\cdot\mathbf{n}=-\sin\Theta\cos\Psi, \ (\mathbf{s}_x \text{ to be defined below}) \quad (A7)$$

$$\mathbf{s}_x\cdot\hat{q}_i=-\sin\Theta_i\cos\Psi. \quad (A8)$$

Three-body states are specified by supplying (a) the two coordinates on the Dalitz plot and so determining the configuration in the production plane; and (b) Euler angles (α,β,γ) to specify the orientation of the production plane. Thus if $(\mathbf{b}_x,\mathbf{b}_y,\mathbf{b}_z)$ are unit vectors along "body-fixed" axes and $(\mathbf{s}_x,\mathbf{s}_y,\mathbf{s}_z)$ are the corresponding space-fixed axes, we have

$$(\mathbf{b}_x,\mathbf{b}_y,\mathbf{b}_z)=R_{\alpha\beta\gamma}{}^{-1}(\mathbf{s}_x,\mathbf{s}_y,\mathbf{s}_z),$$

with

$$R_{\alpha\beta\gamma}=e^{-i\alpha J_x}e^{-i\beta J_y}e^{-i\gamma J_z}.$$

Thus $\cos\beta=(\mathbf{b}_z\cdot\mathbf{s}_z)$, $\sin\beta\cos\alpha=(\mathbf{b}_x\cdot\mathbf{s}_x)$, $-\sin\beta\cos\gamma=(\mathbf{b}_z\cdot\mathbf{s}_x)$.

For the study of production processes, it is convenient to choose $\mathbf{s}_z$ parallel to $\hat{q}_A$ and $\mathbf{s}_x$ arbitrary. The production cross section is independent of the Euler angle γ. Standard body-fixed systems are as follows: (1) a "normal" system with $0Z$ normal to the plane of production and $0X$ in the direction of one of the outgoing particles, say, $\hat{q}_i$: $(\alpha,\beta,\gamma)=(\Phi,\Theta,\Psi)$; (2) the "$k(ij)$" system with $0Z$ parallel to $\hat{q}_k$ and $0X$ on the plane of $\hat{q}_k$ and $\hat{q}_A$; $(\alpha,\beta,\gamma)=(\Phi_i,\Theta_i,\Psi)$. These systems are connected by rotations through known angles and the azimuthal wave functions for given J are related through rotation matrices of these angles.

Thus, we define three-body states by $|\hat{q}_1,\hat{q}_2,\hat{q}_3\rangle$ or, for example, $|\omega_{12}^2,\omega_{23}^2,\Theta_3,\Phi_3\rangle$, or, using the linear relation between $\cos\theta_3$ and ω_{23}^2, for fixed ω_{12}^2, $|\omega_{12}^2,\cos\theta_3,\Theta_3,\Phi_3\rangle$. Integrals over three-body phase space are given by

$$\int\frac{d^3q_1}{2\omega_1}\frac{d^3q_2}{2\omega_2}\frac{d^2q_3}{2\omega_3}\delta(E-\sum\omega_i)\delta(\sum q_i) =\frac{1}{32s}\int d(\cos\Theta_3)d\Phi_3d\Psi d\omega_{12}{}^2d\omega_{23}{}^2 \quad (A9)$$

$$=\int\frac{q_{12}q_3}{16E\omega_{12}}d\omega_{12}{}^2d(\cos\Theta_3)d\Phi_3d\Psi d(\cos\theta_3). \quad (A10)$$

The modifications to go to alternative coordinates are obvious. For a general choice of Euler angles (α,β,γ) one has $d(\cos\beta)d\alpha d\gamma$. It is convenient to associate the (Φ_3,Θ_3,Ψ) system with the $\cos\theta_3$ decomposition in order to use $\hat{q}_3$ as a common quantization axis.

We can now develop unit projection operators for three-body states, using the phase-space transformations (A9), (A10) and the orthonormal property of the rotation matrices,

$$\int_0^{2\pi}d\alpha\int_{-1}^{1}d(\cos\beta)\int_0^{2\pi}d\gamma D_{m_1'm_1}{}^{j_i*}(\alpha\beta\gamma) \times D_{m_2'm_2}{}^{j_2}(\alpha\beta\gamma)=\delta_{m_1'm_2'}\delta_{m_1m_2}\delta_{j_1j_2}\frac{8\pi^2}{2j_1+1}. \quad (A11)$$

Thus,

$$J(3)\equiv\int|\mathbf{q}_1,\mathbf{q}_2,\mathbf{q}_3\rangle\frac{d^3q_1}{2\omega_1}\frac{d^3q_2}{2\omega_2}\frac{d^3q_3}{2\omega_3}\times\delta(E-\sum\omega_i)\delta^3(\sum\mathbf{q}_i)\langle\mathbf{q}_1\mathbf{q}_2\mathbf{q}_3| \quad \text{(A12)}$$

$$=\sum_{J\Lambda M\lambda_i}\left(\frac{8\pi^2}{2J+1}\right)\int\frac{d\omega_{12}{}^2d\omega_{23}{}^2}{32s}\times|s;\omega_{12}{}^2,\omega_{23}{}^2,J\Lambda\lambda_iM\rangle\langle s;\omega_{12}{}^2,\omega_{23}{}^2,J\Lambda\lambda_iM|\,; \quad \text{(A13)}$$

(analysis by transversity spin components)

$$=\sum_{J\mu m\mu_i}\left(\frac{8\pi^2}{2J+1}\right)\int\frac{d\omega_{12}{}^2d\omega_{23}{}^2}{32s}\times|s;\omega_{12}{}^2,\omega_{23}{}^2,J\mu\mu_im\rangle\langle s;\omega_{12}{}^2,\omega_{23}{}^2,J\mu\mu_im|\,; \quad \text{(A14)}$$

(analysis with quantization axis in direction $\hat{q}_i$ and helicity components for spin)

$$=\sum_{J\mu m\mu_i}\left(\frac{8\pi^2}{2J+1}\right)\int\frac{1}{32s}\left(\frac{2Eq_{12}q_3}{\omega_{12}}\right)d(\cos\theta_3)d\omega_{12}{}^2\times|s;\omega_{12}{}^2,\cos\theta_3;J\mu\mu_im\rangle\langle s;\omega_{12}{}^2,\cos\theta_3;J\mu\mu_im|\,. \quad \text{(A15)}$$

We introduce the second angular momentum analysis through the definition

$$|s,\omega_{12}{}^2j_{12};J\mu\mu_3m\rangle=\tfrac{1}{4}(q_{12}q_3/E\omega_{12})^{1/2}((2j_{12}+1)/4\pi)^{1/2}\times\int d(\cos\theta_3)d_{m_{12}\mu}{}^{j_{12}}(\theta_3)\,|s;\omega_{12}{}^2,\cos\theta_3;J\mu\mu_3m\rangle, \quad \text{(A16)}$$

with $m_{12}=\mu+\mu_3$. It then follows from the properties of the $d_{ab}{}^{j_{12}}$ that

$$J(3)=\sum_{J\mu m}\sum_{j_{12}m_{12}}\left(\frac{16\pi^3}{2J+1}\right)\int d\omega_{12}{}^2|s;\omega_{12}{}^2;j_{12}m_{12};J\mu m\rangle\times\langle s,\omega_{12}{}^2;j_{12}m_{12};J\mu m|\,. \quad \text{(A17)}$$

The notation in Eqs. (A13) to (A17) is as follows:

J = total angular momentum;
Λ = component of J in direction $\mathbf{n}$;
λ_i = component of spin of particle i in direction $\mathbf{n}$.

[For $(\pi,\pi,N)=(1,2,3)$ we only need λ_3.]

μ = component of J in direction $\hat{q}_i$;
μ_i = helicity of particle i in the over-all c.m. frame (we only need refer to μ_3);
m = component of J along space-fixed Z axis. Choosing this to be $\hat{q}_A$, m is the initial nucleon helicity;
j_{12} = total angular momentum of the 1, 2 subsystem;
m_{12} = component of j_{12} along $\hat{q}_3$.

The basis states of (A13) and (A14) are related through transformations of the form $D_{\Lambda\mu}{}^J(\chi,\pi/2,0)$, with $\chi=\rho_i$ previously defined, together with similar transformations $D_{\lambda_i\mu_i}{}^{1/2}(\chi',\pi/2,0)$ for the change of spin quantization.

One requires the second angular momentum decomposition for the $\pi(\pi N)$ partition as well as for the $(\pi\pi)N$ partition discussed above. In order to discuss the production of πN isobars with specific angular momentum properties in their own rest system, one has to describe the nucleon spin using the helicity components ν_i in the same two-body c.m. system. These are related to the helicity components μ_i in the over-all c.m. frame through the Wick rotations.[7] The transformation matrices are of the form $d_{\lambda_i\nu_i}{}^{1/2}(\beta)$ with $\beta=\beta_{32}$ for the 1(23) partition, $\beta=\beta_{31}$ for the 2(31) partition, the Wick angles β_{32} and β_{31} being defined below. The Wick angle β_{32} express the relation between spin components in the (23) c.m. system taken in the direction $\hat{q}_{23}$ and spin components in the over-all c.m. system taken in the direction $\hat{q}_3$. In the nonrelativistic approximation, the relative motion of the two reference systems has no effect and β_{32} equals the angle between $\hat{q}_{23}$ and $\hat{q}_3$, $\chi_2-\theta_1$ (see Fig. 3). Relativistic effects introduce an additional rotation Ω_{32}:

$$\beta_{32}=\chi_2-\theta_1+\Omega_{32}. \quad \text{(A18)}$$

The angles Ω_{32} were introduced by Stapp[51] and are discussed in Ref. 5. In the present notation, the Stapp formula becomes

$$\sin\Omega_{32}=\frac{V_1V_{23}\sin\theta_1(1+\gamma_1+\gamma_{23}+\gamma_N)}{(1+\gamma_1)(1+\gamma_{23})(1+\gamma_N)}, \quad \text{(A19)}$$

with $V_{23}=q_{23}/M$, $V_1=q_1/\omega_{23}$, $\gamma_\alpha=[1+V_\alpha{}^2]^{1/2}$, ($\alpha=23$, 1), $\gamma_N=\omega_3/M$. It is easily verified[5] that for $T_\pi\lesssim1$ GeV, Ω_{32} remains small; for example, taking $T_\pi=1$ GeV and $\omega_{23}=1.236$ GeV, $\Omega_{32}<9°$. Thus we are justified in making the nonrelativistic spin approximation.

We finally list certain kinematic relations among alternative variables on the Dalitz plot:

$$\omega_{23}{}^2=E^2+m_1{}^2-2E\omega_1, \quad \text{(A20)}$$

$$\omega_1{}^2=q_1{}^2+m_1{}^2, \text{ (the } m_i \text{ are the masses of final particle 1, 2, 3)} \quad \text{(A21)}$$

$$q_{23}{}^2=[\omega_{23}{}^2-(m_2+m_3)^2][\omega_{23}{}^2-(m_2-m_3)^2]/4\omega_{23}{}^2, \quad \text{(A22)}$$

$$q_1{}^2=[E^2-(m_1+\omega_{23})^2][E^2-(m_1-\omega_{23})^2]/4E^2, \quad \text{(A23)}$$

$$\omega_{23}{}^2=(1/2\omega_{12}{}^2)[(E^2-m_3{}^2)(m_2{}^2-m_1{}^2)+\omega_{12}{}^2(E^2+m_1{}^2+m_2{}^2+m_3{}^2-\omega_{12}{}^2)-4Eq_3\omega_{12}q_{12}\cos\theta_3]. \quad \text{(A24)}$$

Formulas for the angles χ_i in terms of the c.m. momenta q_i follow from the triangle of momentum [Fig. 3(a)]:

$$\cos\chi_1=(q_1{}^2-q_2{}^2-q_3{}^2)/2q_2q_3. \quad \text{(A25)}$$

Formulas for the Wick angles β_{ij} come from applying

[51] H. P. Stapp, Phys. Rev. **163**, 425 (1957).

spherical trigonometry to the Wick triangle[7] [Fig. 3(b)] with

$\cos\zeta_3=\gamma$ (the Lorentz factor) for the (12) system in the over-all c.m. system,

$\cos\xi_{12}=\gamma$ for particle 1 in the (12) c.m. system,
$\cos\epsilon_3=\gamma$ for particle 3 in the over-all c.m. system.
Additional formulas are obtained by permutation.

APPENDIX B: ANALYSIS OF PRODUCTION ANGULAR DISTRIBUTIONS

We briefly recapitulate the analysis of Arnold and Uretsky[10] in order to clarify the remarks on parity eigenstates, correct one or two numerical factors, and recast the formulas for the present purpose. The object is to develop a formalism for interpreting experimental information on $\partial\sigma/\partial\cos\Theta_i$. The starting point is the first angular momentum decomposition of Eq. (2.2). We follow the notation of Sec. II.

Under the parity operation helicities change sign, transversities do not. Applying this and properties of rotation matrices, we deduce from parity conservation that

$$\langle s,\omega_{ij}^2;\,\Lambda\lambda\,|\,T_J(s)\,|\,m\rangle = \eta\eta'(-1)^{j+\Lambda}\langle s,\omega_{ij}^2;\,\Lambda\lambda\,|\,T_J(s)\,|\,-m\rangle, \quad \text{(B1)}$$

where the intrinsic parity factors η and η' have the values -1 and $+1$. By considering the effect of the parity operator on a final state,

$$P\,|\,s,\omega_{ij}^2;\,\alpha\beta\gamma;\,\lambda\rangle = \sum D_{M\Lambda}{}^J(\alpha\beta\pi+\gamma)e^{-i\lambda\pi}\,|\,s,\omega_{ij}^2,\Lambda M;\,\lambda\rangle = \sum(-1)^{\Lambda-\lambda}D_{M\Lambda}{}^J(\alpha\beta\gamma)\,|\,s,\omega_{ij}^2,\Lambda M;\,\lambda\rangle, \quad \text{(B2)}$$

we conclude that the parity of the state with total transversity Λ and nucleon transversity λ is $(-1)^{\Lambda-\lambda}$. Thus the formula for scattering from a state of definite parity $(\pm)$ is

$$T_\lambda{}^{m\pm}(s,\omega_1,\omega_2;\,\Phi,\Theta,\Psi)=\sum_{J=1/2}^{\infty}\sum_{\Lambda=-J}^{J}\left(\frac{2J+1}{4\pi}\right)^{1/2} \times D_{\Lambda m}{}^J(\Phi,\Theta,\Psi)T_{J\Lambda}{}^{m\lambda}(\omega_1,\omega_2)\tfrac{1}{2}[1\pm(-1)^{\Lambda-\lambda}]. \quad \text{(B3)}$$

We note that λ serves to label the parity.

The AU analysis can now be followed through to deduce the spherical harmonic expansion for the production intensity W off an unpolarized target (cross section apart from a kinematic factor depending only on s):

$$W(\Theta,\Phi,\omega_1,\omega_2)=\sum_{jM}\left(\frac{2j+1}{4\pi}\right)^{1/2} \times Y_j{}^{M*}(\Theta,\Phi)W_M{}^j(s,\omega_1,\omega_2). \quad \text{(B4)}$$

Here,

$$W_M{}^j=\frac{1}{2\pi}\sum_{JJ',\Lambda\Lambda'}\langle J\Lambda,J'\Lambda'\rangle\,G_M{}^j(J\Lambda,J'\Lambda'), \quad \text{(B5)}$$

with the combinatorial factor $G_M{}^j$ given by

$$G_M{}^j=2\pi(2J+1)^{1/2}(2J'+1)^{1/2} \times(-1)^{\Lambda'-1/2}[1-(-1)^{\Lambda+\Lambda'+j}]\delta_{\Lambda-\Lambda',M} \times\begin{pmatrix}J & J' & j\\ \Lambda & -\Lambda' & \Lambda'-\Lambda\end{pmatrix}\begin{pmatrix}J & J' & j\\ \frac{1}{2} & -\frac{1}{2} & 0\end{pmatrix}, \quad \text{(B6)}$$

and the dynamical coefficients $\langle J\Lambda,J'\Lambda'\rangle$ given by

$$\langle J\Lambda,J'\Lambda'\rangle=\sum_\lambda B_{J\Lambda}{}^\lambda(\omega_1,\omega_2)B_{J'\Lambda'}{}^{\lambda*}=\langle J'\Lambda',J\Lambda\rangle^*. \quad \text{(B7)}$$

The dependence on the initial helicity m, which can take the values $\pm\frac{1}{2}$, has been eliminated through the relation $B_{J\Lambda}{}^{m\lambda}=(-1)^{J+\Lambda}B_{J\Lambda}{}^{-m\lambda}$, (B1). Quantities are now to be understood to have $m=+\frac{1}{2}$. In the present application, averages of the coefficients (B7) over the Dalitz plot are employed. Since presently available information relates to $\partial\sigma/\partial\cos\Theta_i$, one has to rotate axes and AU give the formulas

$$\bar{W}(\Theta_i,\Phi_i)=\sum_{jM}\left(\frac{2j+1}{4\pi}\right)^{1/2}Y_j{}^{M*}(\Theta_i,\Phi_i)\bar{W}_M{}^j, \quad \text{(B8)}$$

with the $\bar{W}_M{}^j$ related to the previously defined $W_M{}^j$'s in the normal system by

$$\bar{W}_M{}^j=\sum_{M'=-J}^{J}W_{M'}{}^jD_{M'M}{}^j(0,\pi/2,0). \quad \text{(B9)}$$

This simple form results from choosing the x axis of the normal system to lie along the direction $\hat{q}_i$. If it lay instead along the direction $\hat{q}_j$, the rotation matrix would be $D_{M'M}{}^j(\pm\chi_k,\pi/2,0)$ and this extra factor would have to be taken inside the average over the Dalitz plot. Coefficients for (Θ_i,Φ_i) analysis for different values of i are thus not simply related. AU finally give the simple formula, obtained by averaging over Φ_i,

$$\frac{\partial\sigma}{\partial(\cos\Theta_i)}\equiv\bar{W}(\Theta_i)=\sum(2j+1)P_j(\cos\Theta_i)(2\pi\bar{W}_0{}^j). \quad \text{(B10)}$$

These authors give the special formulas resulting when only states with $J\leqslant\frac{3}{2}$ contribute which is also the assumption of the present analysis. They denote the amplitude for production to states $J=\frac{1}{2}$, Λ by $B_{2\Lambda}$ and those for production to $J=\frac{3}{2}$, Λ by $C_{2\Lambda}$. Note that the formula for the $G_M{}^J$'s does not depend on the nucleon transversity λ. There is thus a "parity doubling" through the formulas, i.e., each term in the sum below has two contributions.

The formulas for the relevant $W_m{}^j$ in the normal

system are

$$
\begin{aligned}
W_0{}^0 &= |B_1|^2+|B_{-1}|^2+|C_3|^2 \\
&\quad +|C_1|^2+|C_{-1}|^2+|C_{-3}|^2, \\
W_1{}^1 &= -\tfrac{1}{3}[\sqrt{3}C_3B_1{}^*+C_1B_{-1}{}^*-\sqrt{2}B_1B_{-1}{}^* \\
&\quad -\sqrt{3}B_{-1}C_{-3}{}^*-B_1C_{-1}{}^*] \\
&\quad +\tfrac{1}{5}(\sqrt{\tfrac{2}{3}})[C_3C_1{}^*+(2/\sqrt{3})C_1C_{-1}{}^*+C_{-1}C_{-3}{}^*], \\
W_0{}^2 &= \tfrac{1}{5}[|C_1|^2+|C_{-1}|^2-|C_3|^2-|C_{-3}|^2] \\
&\quad +\tfrac{1}{5}\sqrt{2}[B_1C_1{}^*+C_1B_1{}^*-B_{-1}C_{-1}{}^*-C_{-1}B_{-1}{}^*], \\
W_2{}^2 &= -\tfrac{1}{5}\sqrt{2}[C_3C_{-1}{}^*+C_1C_{-3}{}^*] \\
&\quad +\tfrac{2}{5}[B_1C_{-3}{}^*-C_3B_{-1}{}^*], \\
W_1{}^3 &= -(6/35)[C_3C_1{}^*+C_{-1}C_{-3}{}^*-\sqrt{3}C_1C_{-1}{}^*], \\
W_3{}^3 &= -6/(7\sqrt{5})C_3C_{-3}{}^*.
\end{aligned}
\tag{B11}
$$

The corresponding terms with negative M are given in terms of the above by the relation

$$W_{-M}{}^j = W_M{}^{j*}(-1)^M. \tag{B12}$$

Terms with odd $j+M$ vanish. The corresponding formulas relating to $d\sigma/d(\cos\Theta_i)$ for the $\bar{W}_M{}^j$'s are

$$
\begin{aligned}
\bar{W}_0{}^0 &= |B_1|^2+|B_{-1}|^2+|C_3|^2+|C_1|^2 \\
&\quad +|C_{-1}|^2+|C_{-3}|^2\equiv A_0, \\
\bar{W}_0{}^1 &= \tfrac{2}{3}\,\mathrm{Re}\{B_1{}^*B_{-1}-(\sqrt{\tfrac{3}{2}})(B_1{}^*C_3-B_{-1}{}^*C_{-3}) \\
&\quad -\tfrac{1}{2}\sqrt{2}(C_1B_{-1}{}^*-B_1C_{-1}{}^*)+(3/5\sqrt{3}) \\
&\quad \times[C_3C_1{}^*+(2/\sqrt{3})C_1C_{-1}{}^*+C_{-1}C_{-3}{}^*]\}\equiv\tfrac{1}{3}A_1, \\
\bar{W}_0{}^2 &= -\tfrac{1}{10}\,\mathrm{Re}\{|C_1|^2+|C_{-1}|^2-|C_3|^2-|C_{-3}|^2 \\
&\quad +2\sqrt{3}[C_3C_{-1}{}^*+C_1C_{-3}{}^*]+2\sqrt{2}[B_1C_1{}^*-B_{-1}C_{-1}{}^*] \\
&\quad -2(\sqrt{6})[B_1C_{-3}{}^*-C_3B_{-1}{}^*]\}\equiv\tfrac{1}{5}A_2, \\
\bar{W}_0{}^3 &= (3/7)\,\mathrm{Re}\{-C_3C_{-3}{}^*+\tfrac{1}{5}\sqrt{3}[C_3C_1{}^* \\
&\quad +C_{-1}C_{-3}{}^*-\sqrt{3}C_1C_{-1}{}^*]\}\equiv(1/7)A_3.
\end{aligned}
\tag{B13}
$$

Note that we have introduced the quantities $A_J=(2j+1)\bar{W}_0{}^j$ which are the actual coefficients of $P_J(\cos\Theta_i)$.

It is convenient to introduce a more mnemonic notation which emphasizes the J^P assignments of the spin components. We therefore write in an obvious notation

$$
\begin{bmatrix} C_3 \\ C_1 \\ C_{-1} \\ C_{-3} \end{bmatrix}
=\uparrow\begin{bmatrix} D_3{}^3 \\ P_3{}^1 \\ D_3{}^{-1} \\ P_3{}^{-3} \end{bmatrix}
+\downarrow\begin{bmatrix} P_3{}^3 \\ D_3{}^1 \\ P_3{}^{-1} \\ D_3{}^{-3} \end{bmatrix}
\tag{B14}
$$

$$
\begin{bmatrix} B_1 \\ B_{-1} \end{bmatrix}
=\uparrow\begin{bmatrix} P_1{}^1 \\ S_1{}^{-1} \end{bmatrix}
+\downarrow\begin{bmatrix} S_1{}^1 \\ P_1{}^{-1} \end{bmatrix},
$$

where $\uparrow\downarrow$ denotes $\lambda=\pm\frac{1}{2}$. We can further exploit a symmetry of the $G_M{}^j$ coefficients according to which terms always occur in pairs:

$$\langle J\Lambda,J'\Lambda'\rangle+(-1)^{J+J'+j+1+\Lambda-\Lambda'}\langle J-\Lambda,J'-\Lambda'\rangle.$$

We therefore define abstract 2-vectors:

$$
\begin{aligned}
P_1 &\equiv \begin{bmatrix} P_1{}^1 \\ -P_1{}^{-1} \end{bmatrix}, \qquad
S_1 \equiv \begin{bmatrix} S_1{}^{-1} \\ -S_1{}^1 \end{bmatrix}, \\
D_3{}^{(3)} &\equiv \begin{bmatrix} D_3{}^3 \\ D_3{}^{-3} \end{bmatrix}, \qquad
D_3{}^{(1)} \equiv \begin{bmatrix} D_3{}^{-1} \\ D_3{}^1 \end{bmatrix}, \\
P_3{}^{(3)} &\equiv \begin{bmatrix} P_3{}^{-3} \\ P_3{}^3 \end{bmatrix}, \qquad
P_3{}^{(1)} \equiv \begin{bmatrix} P_3{}^1 \\ P_3{}^{-1} \end{bmatrix}.
\end{aligned}
\tag{B15}
$$

We can then rewrite the formulas for the A_J in terms of these quantities with expressions such as

$$D_3{}^{(3)}\cdot P_3{}^{(3)*}\equiv D_3{}^3P_3{}^{-3*}+D_3{}^{-3}P_3{}^{3*},$$

i.e., interpreted as a scalar product.

It turns out that more transparent formulas result if alternative spin combinations are employed. Define s_1, p_1, $d_3{}^{(1)}$, $d_3{}^{(2)}$, $p_3{}^{(1)}$, $p_3{}^{(2)}$ through the formulas

$$
\begin{aligned}
S_1 &= s_1, \\
P_1 &= p_1, \\
D_3{}^{(3)} &= \tfrac{1}{2}d_3{}^{(1)}+\tfrac{1}{2}\sqrt{3}d_3{}^{(2)}, \\
D_3{}^{(1)} &= \tfrac{1}{2}\sqrt{3}d_3{}^{(1)}-\tfrac{1}{2}d_3{}^{(2)},
\end{aligned}
\tag{B16}
$$

with similar formulas for the $p_3{}^{(i)}$ in terms of $P_3{}^{(j)}$. As a result, we obtain

$$
\begin{aligned}
A_0 &= |s_1|^2+|p_1|^2+|d_3{}^{(3)}|^2+|d_3{}^{(2)}|^2 \\
&\quad +|p_3{}^{(1)}|^2+|p_3{}^{(2)}|^2, \\
A_1 &= 2\,\mathrm{Re}\{p_1{}^*\cdot s_1-\sqrt{2}(p_1{}^*\cdot d_3{}^{(2)}-s_1{}^*p_3{}^{(2)}) \\
&\quad +\tfrac{3}{5}(p_3{}^{(1)*}\cdot d_3{}^{(1)}-\tfrac{1}{3}p_3{}^{(2)*}\cdot d_3{}^{(2)})\}, \\
A_2 &= \mathrm{Re}\{|d_3{}^{(2)}|^2-|d_3{}^{(1)}|^2+|p_3{}^{(2)}|^2-|p_3{}^{(1)}|^2 \\
&\quad +2\sqrt{2}(p_1{}^*\cdot p_3{}^{(2)}-s_1{}^*\cdot d_3{}^{(2)})\}, \\
A_3 &= -3\,\mathrm{Re}\{\tfrac{2}{5}p_3{}^{(1)*}\cdot d_3{}^{(1)}+(6/5)p_3{}^{(2)*}\cdot d_3{}^{(2)}\}.
\end{aligned}
\tag{B17}
$$

Note the relations

$$
\begin{aligned}
A_0+A_2 &= |s_1-\sqrt{2}d_3{}^{(2)}|^2+|p_1+\sqrt{2}p_3{}^{(2)}|^2, \\
A_1+A_3 &= 2\,\mathrm{Re}(s_1-\sqrt{2}d_3{}^{(2)})^*\cdot(p_1+\sqrt{2}p_3{}^{(2)}), \\
A_0+A_1+A_2+A_3 &= |s_1+p_1-\sqrt{2}d_3{}^{(2)}+\sqrt{2}p_3{}^{(2)}|^2.
\end{aligned}
\tag{B18}
$$

We have now achieved compact formulas which give in particular a simple form for coefficient A_2 in terms of $J=\frac{3}{2}$ components which contribute, respectively, positive and negative curvature.